Diquat Derivatives: Highly Active, Two-Dimensional Nonlinear Optical Chromophores with Potential Redox Switchability

ARTICLE *in* JOURNAL OF THE AMERICAN CHEMICAL SOCIETY · AUGUST 2010

Impact Factor: 12.11 · DOI: 10.1021/ja103289a · Source: PubMed

10 AUTHORS, INCLUDING:

Bruce Brunschwig
California Institute of Technology
202 PUBLICATIONS **7,669** CITATIONS
SEE PROFILE

Jesús Orduna
Spanish National Research Council
199 PUBLICATIONS **3,154** CITATIONS
SEE PROFILE

J|A|C|S ARTICLES

Published on Web 07/09/2010

Diquat Derivatives: Highly Active, Two-Dimensional Nonlinear Optical Chromophores with Potential Redox Switchability

Benjamin J. Coe,*,† John Fielden,† Simon P. Foxon,† James A. Harris,† Madeleine Helliwell,† Bruce S. Brunschwig,‡ Inge Asselberghs,§ Koen Clays,§ Javier Garín,|| and Jesús Orduna||

School of Chemistry, University of Manchester, Oxford Road, Manchester M13 9PL, U.K., Molecular Materials Research Center, Beckman Institute, MC 139-74, California Institute of Technology, 1200 East California Boulevard, Pasadena, California 91125, Department of Chemistry, University of Leuven, Celestijnenlaan 200D, B-3001 Leuven, Belgium, and Departamento de Química Orgánica, ICMA, Universidad de Zaragoza-CSIC, E-50009 Zaragoza, Spain

Received April 19, 2010; E-mail: b.coe@manchester.ac.uk.

Abstract: In this article, we present a detailed study of structure−activity relationships in diquaternized 2,2′-bipyridyl (diquat) derivatives. Sixteen new chromophores have been synthesized, with variations in the amino electron donor substituents, π-conjugated bridge, and alkyl diquaternizing unit. Our aim is to combine very large, two-dimensional (2D) quadratic nonlinear optical (NLO) responses with reversible redox chemistry. The chromophores have been characterized as their PF_6^- salts by using various techniques including electronic absorption spectroscopy and cyclic voltammetry. Their visible absorption spectra are dominated by intense $\pi \rightarrow \pi^*$ intramolecular charge-transfer (ICT) bands, and all show two reversible diquat-based reductions. First hyperpolarizabilities β have been measured by using hyper-Rayleigh scattering with an 800 nm laser, and Stark spectroscopy of the ICT bands affords estimated static first hyperpolarizabilities β_0. The directly and indirectly derived β values are large and increase with the extent of π-conjugation and electron donor strength. Extending the quaternizing alkyl linkage always increases the ICT energy and decreases the $E_{1/2}$ values for diquat reduction, but a compensating increase in the ICT intensity prevents significant decreases in Stark-based β_0 responses. Nine single-crystal X-ray structures have also been obtained. Time-dependent density functional theory clarifies the molecular electronic/optical properties, and finite field calculations agree with polarized HRS data in that the NLO responses of the disubstituted species are dominated by 'off-diagonal' β_{zyy} components. The most significant findings of these studies are: (i) β_0 values as much as 6 times that of the chromophore in the technologically important material (*E*)-4′-(dimethylamino)-*N*-methyl-4-stilbazolium tosylate; (ii) reversible electrochemistry that offers potential for redox-switching of optical properties over multiple states; (iii) strongly 2D NLO responses that may be exploited for novel practical applications; (iv) a new polar material, suitable for bulk NLO behavior.

Introduction

In addition to purely academic incentives, a wealth of diverse applications such as advanced telecommunications and biological imaging makes organic nonlinear optical (NLO) materials of great current interest.[1] For example, NLO effects can allow the exchange of information between laser beams and thus may lead to the creation of all-optical computing devices. For molecular species, quadratic (*second-order*) NLO behavior arises from the first hyperpolarizability β that translates into $\chi^{(2)}$ in bulk materials. In order to achieve nonzero values of both β and $\chi^{(2)}$, noncentrosymmetric structures are essential.

Synthetic chemistry drives much fundamental NLO research, which has involved a wide variety of compounds, including organic salts. An important feature of salts is that counterion variations can be used to modify crystal packing, potentially giving polar structures showing quadratic NLO effects such as second harmonic generation (SHG) and linear electrooptic behavior. Solubility can also be thus tuned, having implications for imaging applications. Other attractive aspects of crystalline salts are their inherently greater stabilities and higher chromophore number densities when compared with alternative NLO materials such as poled polymers. In this context, special attention has been given to compounds such as (*E*)-4′-(dimethylamino)-*N*-methyl-4-stilbazolium tosylate (DAST)[2] and related species.[3] Notably, crystals of DAST have recently been

† University of Manchester.
‡ California Institute of Technology.
§ University of Leuven.
|| Universidad de Zaragoza.

(1) (a) Zyss, J. *Molecular Nonlinear Optics: Materials, Physics and Devices*; Academic Press: Boston, 1994. (b) Bosshard, Ch.; Sutter, K.; Prêtre, Ph.; Hulliger, J.; Flörsheimer, M.; Kaatz, P.; Günter, P. *Advances in Nonlinear Optics*; Organic Nonlinear Optical Materials, Vol. 1; Gordon & Breach: Amsterdam, The Netherlands, 1995. (c) *Nonlinear Optics of Organic Molecules and Polymers*; Nalwa, H. S., Miyata, S., Eds.; CRC Press: Boca Raton, FL, 1997. (d) Marder, S. R. *Chem. Commun.* **2006**, 131–134. (e) *Nonlinear Optical Properties of Matter: From Molecules to Condensed Phases*; Papadopoulos, M. G.; Leszczynski, J.; Sadlej, A. J., Eds.; Springer: Dordrecht, 2006. (f) Kuzyk, M. G. *J. Mater. Chem.* **2009**, *19*, 7444–7465.

 10.1021/ja103289a

commercialized for terahertz (THz) wave generation via nonlinear frequency mixing.[4] Terahertz radiation lies between the microwave and IR regions and has many applications including security scanning, biomedical analysis, and space communications.[5] When compared with semiconductors such as GaAs, organic materials with large $\chi^{(2)}$ values can produce broader bandwidths and also allow higher-power outputs without damage. The major limitation of DAST is a gap in the spectrum produced between 0.9 and 1.3 THz,[5c] and it is likely that the versatility of organic synthesis can be used to produce better materials giving more complete spectral coverage and/or superior crystal growth or stability properties.

Molecules with large β responses contain π-electron donor (π-ED) and acceptor (π-EA) groups linked via polarizable π-systems, with pyridinium rings being strong π-EAs in stilbazolium dyes. Such chromophores also show intense $\pi \rightarrow \pi^*$ intramolecular charge-transfer (ICT) absorptions. Hyperpolarizabilities are tensor quantities that can have several nonzero components. Although most NLO chromophores have simple one-dimensional (1D) dipolar structures, multidimensional species including 2D dipoles[6] and 2D or 3D octupoles[7] are also very interesting. Such molecules offer significant potential advantages over their 1D counterparts, including increased NLO responses without undesirable losses of visible transparency. In V-shaped species, the presence of more than one significant component of β is important in various ways, for example preventing reabsorption of harmonic light due to its polarization being perpendicular to the ICT transition dipole moment (μ_{12}) and facilitating phase-matching between the fundamental and harmonic waves in SHG.[6a]

We have previously studied salts of stilbazolium-type chromophores with *N*-arylpyridinium groups[8] and also related *N*-methylbenzothiazolium species.[9] Two salts have been discovered that crystallize in the acentric space group *Cc* and have powder SHG efficiencies similar to that of DAST (using a 1907 nm laser). The compound (*E*)-4′-(dimethylamino)-*N*-phenyl-4-stilbazolium hexafluorophosphate shows polymorphism,[10] and Maker fringe SHG measurements on large, single crystals of the active form afford a huge diagonal NLO susceptibility of $d_{111} \approx 290$ pm V^{-1} at 1907 nm (cf., DAST gives $d_{111} \approx 210$

(2) Selected examples: (a) Marder, S. R.; Perry, J. W.; Schaefer, W. P. *Science* **1989**, *245*, 626–628. (b) Marder, S. R.; Perry, J. W.; Yakymyshyn, C. P. *Chem. Mater.* **1994**, *6*, 1137–1147. (c) Lee, O.-K.; Kim, K.-S. *Photonics Sci. News* **1999**, *4*, 9–20. (d) Sohma, S.; Takahashi, H.; Taniuchi, T.; Ito, H. *Chem. Phys.* **1999**, *245*, 359–364. (e) Kaino, T.; Cai, B.; Takayama, K. *Adv. Funct. Mater.* **2002**, *12*, 599–603. (f) Mohan Kumar, R.; Rajan Babu, D.; Ravi, G.; Jayavel, R. *J. Cryst. Growth* **2003**, *250*, 113–117. (g) Geis, W.; Sinta, R.; Mowers, W.; Deneault, S. J.; Marchant, M. F.; Krohn, K. E.; Spector, S. J.; Calawa, D. R.; Lyszczarz, T. M. *Appl. Phys. Lett.* **2004**, *84*, 3729–3731.

(3) Selected examples: (a) Marder, S. R.; Perry, J. W.; Schaefer, W. P. *J. Mater. Chem.* **1992**, *2*, 985–986. (b) Yitzchaik, S.; Marks, T. J. *Acc. Chem. Res.* **1996**, *29*, 197–202. (c) Alain, V.; Blanchard-Desce, M.; Ledoux-Rak, I.; Zyss, J. *Chem. Commun.* **2000**, 353–354. (d) Cariati, E.; Ugo, R.; Cariati, F.; Roberto, D.; Masciocchi, N.; Galli, S.; Sironi, A. *Adv. Mater.* **2001**, *13*, 1665–1668. (e) Abbotto, A.; Beverina, L.; Bradamante, S.; Facchetti, A.; Klein, C.; Pagani, G. A.; Redi-Abshiro, M.; Wortmann, R. *Chem.—Eur. J.* **2003**, *9*, 1991–2007. (f) Kim, H. S.; Lee, S. M.; Ha, K.; Jung, C.; Lee, Y.-J.; Chun, Y. S.; Kim, D.; Rhee, B. K.; Yoon, K. B. *J. Am. Chem. Soc.* **2004**, *126*, 673–682. (g) Yang, Z.; Aravazhi, S.; Schneider, A.; Seiler, P.; Jazbinšek, M.; Günter, P. *Adv. Funct. Mater.* **2005**, *15*, 1072–1076. (h) Ruiz, B.; Yang, Z.; Gramlich, V.; Jazbinšek, M.; Günter, P. *J. Mater. Chem.* **2006**, *16*, 2839–2842. (i) Kim, H. S.; Sohn, K. W.; Jeon, Y.; Min, H.; Kim, D.; Yoon, K. B. *Adv. Mater.* **2007**, *19*, 260–263. (j) Yang, Z.; Jazbinšek, M.; Ruiz, B.; Aravazhi, S.; Gramlich, V.; Günter, P. *Chem. Mater.* **2007**, *19*, 3512–3518. (k) Yang, Z.; Mutter, L.; Stillhart, M.; Ruiz, B.; Aravazhi, S.; Jazbinšek, M.; Schneider, A.; Gramlich, V.; Günter, P. *Adv. Funct. Mater.* **2007**, *17*, 2018–2023. (l) Nunzi, F.; Fantacci, S.; De Angelis, F.; Sgamellotti, A.; Cariati, E.; Ugo, R.; Macchi, P. *J. Phys. Chem. C* **2008**, *112*, 1213–1226. (m) Xu, X.-L.; Qiu, W.-W.; Zhou, Q.; Tang, J.; Yang, F.; Sun, Z.-R.; Audebert, P. *J. Phys. Chem. B* **2008**, *112*, 4913–4917.

(4) Selected examples: (a) Kawase, K.; Mizuno, M.; Sohma, S.; Takahashi, H.; Taniuchi, T.; Urata, Y.; Wada, S.; Tashiro, H.; Ito, H. *Opt. Lett.* **1999**, *24*, 1065–1067. (b) Kawase, K.; Hatanaka, T.; Takahashi, H.; Nakamura, K.; Taniuchi, T.; Ito, H. *Opt. Lett.* **2000**, *25*, 1714–1716. (c) Taniuchi, T.; Okada, S.; Nakanishi, H. *J. Appl. Phys.* **2004**, *95*, 5984–5988. (d) Taniuchi, T.; Ikeda, S.; Okada, S.; Nakanishi, H. *Jpn. J. Appl. Phys.* **2005**, *44*, L652–L654. (e) Schneider, A.; Neis, M.; Stillhart, M.; Ruiz, B.; Khan, R. U. A.; Günter, P. *J. Opt. Soc. Am. B* **2006**, *23*, 1822–1835. (f) Schneider, A.; Stillhart, M.; Günter, P. *Opt. Express* **2006**, *14*, 5376–5384.

(5) (a) *Terahertz Sources and Systems*; Miles, R. E., Harrison, P., Lippens, D., Eds. NATO Science Series II, Vol. 27; Kluwer: Dordrecht, 2001. (b) Ferguson, B.; Zhang, X.-C. *Nat. Mater.* **2002**, *1*, 26–33. (c) McEntee, J. *Chem. World* **2007**, 52–56. (d) http://www.teraview.com.

(6) Selected examples: (a) Wortmann, R.; Krämer, P.; Glania, C.; Lebus, S.; Detzer, N. *Chem. Phys.* **1993**, *173*, 99–108. (b) Moylan, C. R.; Ermer, S.; Lovejoy, S. M.; McComb, I.-H.; Leung, D. S.; Wortmann, R.; Krämer, P.; Twieg, R. J. *J. Am. Chem. Soc.* **1996**, *118*, 12950–12955. (c) Di Bella, S.; Fragalà, I.; Ledoux, I.; Diaz-Garcia, M. A.; Marks, T. J. *J. Am. Chem. Soc.* **1997**, *119*, 9550–9557. (d) Wolff, J. J.; Längle, D.; Hillenbrand, D.; Wortmann, R.; Matschiner, R.; Glania, C.; Krämer, P. *Adv. Mater.* **1997**, *9*, 138–143. (e) Averseng, F.; Lacroix, P. G.; Malfant, I.; Lenoble, G.; Cassoux, P.; Nakatani, K.; Maltey-Fanton, I.; Delaire, J. A.; Aukauloo, A. *Chem. Mater.* **1999**, *11*, 995–1002. (f) Hilton, A.; Renouard, T.; Maury, O.; Le Bozec, H.; Ledoux, I.; Zyss, J. *Chem. Commun.* **1999**, 2521–2522. (g) Lacroix, P. G. *Eur. J. Inorg. Chem.* **2001**, 339–348. (h) Ostroverkhov, V.; Petschek, R. G.; Singer, K. D.; Twieg, R. J. *Chem. Phys. Lett.* **2001**, *340*, 109–115. (i) Di Bella, S.; Fragalà, I.; Ledoux, I.; Zyss, J. *Chem.—Eur. J.* **2001**, *7*, 3738–3743. (j) Yang, M.-L.; Champagne, B. *J. Phys. Chem. A* **2003**, *107*, 3942–3951. (k) Wortmann, R.; Lebus-Henn, S.; Reis, H.; Papadopoulos, M. G. *J. Mol. Struct. (THEOCHEM)* **2003**, *633*, 217–226. (l) Cui, Y.-Z.; Fang, Q.; Huang, Z.-L.; Xue, G.; Yu, W.-T.; Lei, H. *Opt. Mater.* **2005**, *27*, 1571–1575. (m) Rigamonti, L.; Demartin, F.; Forni, A.; Righetto, S.; Pasini, A. *Inorg. Chem.* **2006**, *45*, 10976–10989. (n) Li, H.-P.; Han, K.; Tang, G.; Shen, X.-P.; Wang, H.-T.; Huang, Z.-M.; Zhang, Z.-H.; Bai, L.; Wang, Z.-Y. *Chem. Phys. Lett.* **2007**, *444*, 80–84. (o) Zrig, S.; Koeckelberghs, G.; Verbiest, T.; Andrioletti, B.; Rose, E.; Persoons, A.; Asselberghs, I.; Clays, K. *J. Org. Chem.* **2007**, *72*, 5855–5858. (p) Liu, C.-G.; Qiu, Y.-Q.; Su, Z.-M.; Yang, G.-C.; Sun, S.-L. *J. Phys. Chem. C* **2008**, *112*, 7021–7028. (q) Li, H.-P.; Han, K.; Tang, G.; Li, M.-X.; Shen, X.-P.; Huang, Z.-M. *Mol. Phys.* **2009**, *107*, 1597–1603. (r) Muhammad, S.; Janjua, M. R. S. A.; Su, Z.-M. *J. Phys. Chem. C* **2009**, *113*, 12551–12557.

(7) Selected examples: (a) Verbiest, T.; Clays, K.; Samyn, C.; Wolff, J.; Reinhoudt, D.; Persoons, A. *J. Am. Chem. Soc.* **1994**, *116*, 9320–9323. (b) Zyss, J.; Ledoux, I. *Chem. Rev.* **1994**, *94*, 77–105. (c) Dhenaut, C.; Ledoux, I.; Samuel, I. D. W.; Zyss, J.; Bourgault, M.; Le Bozec, H. *Nature* **1995**, *374*, 339–342. (d) McDonagh, A. M.; Humphrey, M. G.; Samoc, M.; Luther-Davies, B.; Houbrechts, S.; Wada, T.; Sasabe, H.; Persoons, A. *J. Am. Chem. Soc.* **1999**, *121*, 1405–1406. (e) Vance, F. W.; Hupp, J. T. *J. Am. Chem. Soc.* **1999**, *121*, 4047–4053. (f) Wolff, J. J.; Siegler, F.; Matschiner, R.; Wortmann, R. *Angew. Chem., Int. Ed.* **2000**, *39*, 1436–1439. (g) Cho, B. R.; Piao, M. J.; Son, K. H.; Lee, S. H.; Yoon, S. J.; Jeon, S.-J.; Cho, M.-H. *Chem.—Eur. J.* **2002**, *8*, 3907–3916. (h) Le Bouder, T.; Maury, O.; Bondon, O.; Costuas, K.; Amouyal, E.; Ledoux, I.; Zyss, J.; Le Bozec, H. *J. Am. Chem. Soc.* **2003**, *125*, 12284–12299. (i) Maury, O.; Viau, L.; Sénéchal, K.; Corre, B.; Guégan, J.-P.; Renouard, T.; Ledoux, I.; Zyss, J.; Le Bozec, H. *Chem.—Eur. J.* **2004**, *10*, 4454–4466. (j) Maury, O.; Le Bozec, H. *Acc. Chem. Res.* **2005**, *38*, 691–704. (k) Coe, B. J.; Harris, J. A.; Brunschwig, B. S.; Asselberghs, I.; Clays, K.; Garín, J.; Orduna, J. *J. Am. Chem. Soc.* **2005**, *127*, 13399–13410. (l) Le Floc'h, V.; Brasselet, S.; Zyss, J.; Cho, B. R.; Lee, S. H.; Jeon, S.-J.; Cho, M.-H.; Min, K. S.; Suh, M. P. *Adv. Mater.* **2005**, *17*, 196–200. (m) Hennrich, G.; Omenat, A.; Asselberghs, I.; Foerier, S.; Clays, K.; Verbiest, T.; Serrano, J. L. *Angew. Chem., Int. Ed.* **2006**, *45*, 4203–4206. (n) Jeong, M.-Y.; Kim, H. M.; Jeon, S.-J.; Brasselet, S.; Cho, B. R. *Adv. Mater.* **2007**, *19*, 2107–2111. (o) Liu, Y.; Xu, X.; Zheng, F.; Cui, Y. *Angew. Chem., Int. Ed.* **2008**, *47*, 4538–4541. (p) Akdas-Kilig, H.; Roisnel, T.; Ledoux, I.; Le Bozec, H. *New J. Chem.* **2009**, *33*, 1470–1473. (q) Kim, H. M.; Cho, B. R. *J. Mater. Chem.* **2009**, *19*, 7402–7409.

pm V^{-1}).[11] We have hence already produced materials with superior bulk NLO responses when compared with DAST. Our present studies are focused on chromophores featuring the diquaternized 2,2′-bipyridyl (diquat) unit. Except for one brief theoretical study concerning two-photon absorption,[12] the diquat group has not been exploited for NLO purposes previously. We chose this motif because it is a π-EA stronger than a simple pyridinium group, acts as a core for the construction of 2D dipoles, and shows reversible reductions that may be used to switch the optical properties, thus incorporating metal-like properties into low-cost, purely organic chromophores. Preliminary investigations revealed that such molecules exhibit two substantial components of the β tensor, β_{zzz} and β_{zyy};[13] here we describe major extensions of this work that aim to establish structure−activity relationships for these interesting new NLO chromophores.

Experimental Section

Syntheses and Measurements. All of the details relating to the synthetic chemistry, general characterization, X-ray crystallography, hyper-Rayleigh scattering and other physical measurements, and theoretical calculations can be found in the Supporting Information.

Stark Spectroscopy. Full details are in the Supporting Information, while the equations and definitions used are included below because they are integral to the subsequent discussion. A two-state analysis of the ICT transitions gives

$$\Delta\mu_{ab}^2 = \Delta\mu_{12}^2 + 4\mu_{12}^2 \quad (1)$$

where $\Delta\mu_{ab}$ is the dipole-moment change between the diabatic states and $\Delta\mu_{12}$ is the observed (adiabatic) dipole-moment change. The value of μ_{12} can be determined from the oscillator strength f_{os} of the transition by

$$|\mu_{12}| = \left(\frac{f_{os}}{1.08 \times 10^{-5} E_{max}}\right)^{1/2} \quad (2)$$

where E_{max} is the energy of the ICT maximum (in wavenumbers) and μ_{12} is in e·Å. The latter is converted into Debye units upon multiplying by 4.803. The degree of delocalization c_b^2 and electronic coupling matrix element H_{ab} for the diabatic states are given by

$$c_b^2 = \frac{1}{2}\left[1 - \left(\frac{\Delta\mu_{12}^2}{\Delta\mu_{12}^2 + 4\mu_{12}^2}\right)^{1/2}\right] \quad (3)$$

$$\left|H_{ab}\right| = \left|\frac{E_{max}(\mu_{12})}{\Delta\mu_{ab}}\right| \quad (4)$$

If the hyperpolarizability tensor β_0 has only nonzero elements along the ICT direction, then this quantity is given by

$$\beta_0 = \frac{3\Delta\mu_{12}(\mu_{12})^2}{(E_{max})^2} \quad (5)$$

A relative error of ±20% is estimated for the β_0 values derived from the Stark data and using eq 5, while experimental errors of ±10% are estimated for μ_{12}, $\Delta\mu_{12}$, and $\Delta\mu_{ab}$, ±15% for H_{ab} and ±50% for c_b^2. Note that the ±20% uncertainty for the β_0 values is merely statistical and does not account for any errors introduced by two-state extrapolation.

Results and Discussion

Synthetic Studies. Most of the new diquat chromophores **3**−**18** (Figure 1) were prepared in one step from commercial or easily accessible diquat and aldehyde precursors, and isolated as their PF_6^- salts. Knoevenagel condensations between a 2,11/12-dimethyl-diquat derivative and either one equivalent (for monosubstituted (MS) compounds) or 8−20 equiv (for disubstituted (DS) compounds) of the appropriate aldehyde were originally used to access **3** and **11**.[13] This approach also afforded **4**−**7**, **9**, **10**, **12**−**15**, **17**, and **18**. While very large excesses (20 equiv) of aldehyde are necessary to achieve high yields of DS compounds in reactions with 4-(dimethylamino)benzaldehyde, thin-layer chromatography indicates that reactions with (*E*)-4-(dimethylamino)cinnamaldehyde or julolidinyl aldehydes are essentially complete when using only 8−10 equiv. Notably, the synthesis of [**15**][PF_6]$_2$ gave a substantial quantity (∼20% yield) of the corresponding MS compound [**7**][PF_6]$_2$, but no MS products were isolated from the preparations of [**17**][PF_6]$_2$ and [**18**][PF_6]$_2$, despite the use of smaller relative quantities of aldehyde.

Compounds [**3**][PF_6]$_2$ and [**11**][PF_6]$_2$ were purified simply via reprecipitation, exploiting the greatly different solubilities of the corresponding bromide salts in methanol. Using the same method was successful for [**15**][PF_6]$_2$, but not its MS analogue [**7**][PF_6]$_2$. The latter and all the other salts, were purified by column chromatography on silica gel with mixtures of acetone, water and saturated aqueous KNO_3. The isolated yields are relatively low (7−32% for the MS species and 13−51% for their DS counterparts), with substantial quantities of the colored products becoming trapped on the silica gel.

Using the Knoevenagel approach gave unsatisfactory results for **8** or **16**, so these species were prepared by reacting the respective 2,2′-bipyridyl derivatives **1** and **2** (Figure 1) with 1,3-bis(trifluoxy)propane.[14] **1** is a known compound,[15] while **2** was prepared in high yield via a Wadsworth-Emmons reaction between (*E*)-4-(dimethylamino)cinnamaldehyde and 4,4′-bis-[(diethoxyphosphinyl)methyl]-2,2′-bipyridyl.[16] These diquater-

(8) (a) Coe, B. J.; Harris, J. A.; Asselberghs, I.; Clays, K.; Olbrechts, G.; Persoons, A.; Hupp, J. T.; Johnson, R. C.; Coles, S. J.; Hursthouse, M. B.; Nakatani, K. *Adv. Funct. Mater.* **2002**, *12*, 110–116. (b) Clays, K.; Coe, B. J. *Chem. Mater.* **2003**, *15*, 642–648. (c) Coe, B. J.; Harris, J. A.; Asselberghs, I.; Wostyn, K.; Clays, K.; Persoons, A.; Brunschwig, B. S.; Coles, S. J.; Gelbrich, T.; Light, M. E.; Hursthouse, M. B.; Nakatani, K. *Adv. Funct. Mater.* **2003**, *13*, 347–357. (d) Coe, B. J.; Harris, J. A.; Brunschwig, B. S.; Garín, J.; Orduna, J.; Coles, S. J.; Hursthouse, M. B. *J. Am. Chem. Soc.* **2004**, *126*, 10418–10427. (e) Coe, B. J.; Beljonne, D.; Vogel, H.; Garín, J.; Orduna, J. *J. Phys. Chem. A* **2005**, *109*, 10052–10057. (f) Coe, B. J.; Hall, J. J.; Harris, J. A.; Brunschwig, B. S.; Coles, S. J.; Hursthouse, M. B. *Acta Crystallogr., Sect. E* **2005**, *61*, o464–o467.
(9) Coe, B. J.; Harris, J. A.; Hall, J. J.; Brunschwig, B. S.; Hung, S.-T.; Libaers, W.; Clays, K.; Coles, S. J.; Horton, P. N.; Light, M. E.; Hursthouse, M. B.; Garín, J.; Orduna, J. *Chem. Mater.* **2006**, *18*, 5907–5918.
(10) Ruiz, B.; Coe, B. J.; Gianotti, R.; Gramlich, V.; Jazbinšek, M.; Günter, P. *CrystEngComm* **2007**, *9*, 772–776.
(11) Figi, H.; Mutter, L.; Hunziker, C.; Jazbinšek, M.; Günter, P.; Coe, B. J. *J. Opt. Soc. Am. B* **2008**, *25*, 1786–1793.
(12) Zhou, Y.-F.; Meng, F.-Q.; Zhao, X.; Feng, S.-Y.; Jiang, M.-H. *Chem. Phys.* **2001**, *269*, 441–445.
(13) Coe, B. J.; Harris, J. A.; Brunschwig, B. S.; Garín, J.; Orduna, J. *J. Am. Chem. Soc.* **2005**, *127*, 3284–3285.
(14) Lindner, E.; von Au, G.; Eberle, H.-J. *Chem. Ber.* **1981**, *114*, 810–813.
(15) Jang, S.-R.; Lee, C.-C.; Choi, H.-B.; Ko, J. J.; Lee, J.-W.; Vittal, R.; Kim, K.-J. *Chem. Mater.* **2006**, *18*, 5604–5608.
(16) Gillaizeau-Gauthier, I.; Odobel, F.; Alebbi, M.; Argazzi, R.; Costa, E.; Bignozzi, C. A.; Qu, P.; Meyer, G. J. *Inorg. Chem.* **2001**, *40*, 6073–6079.

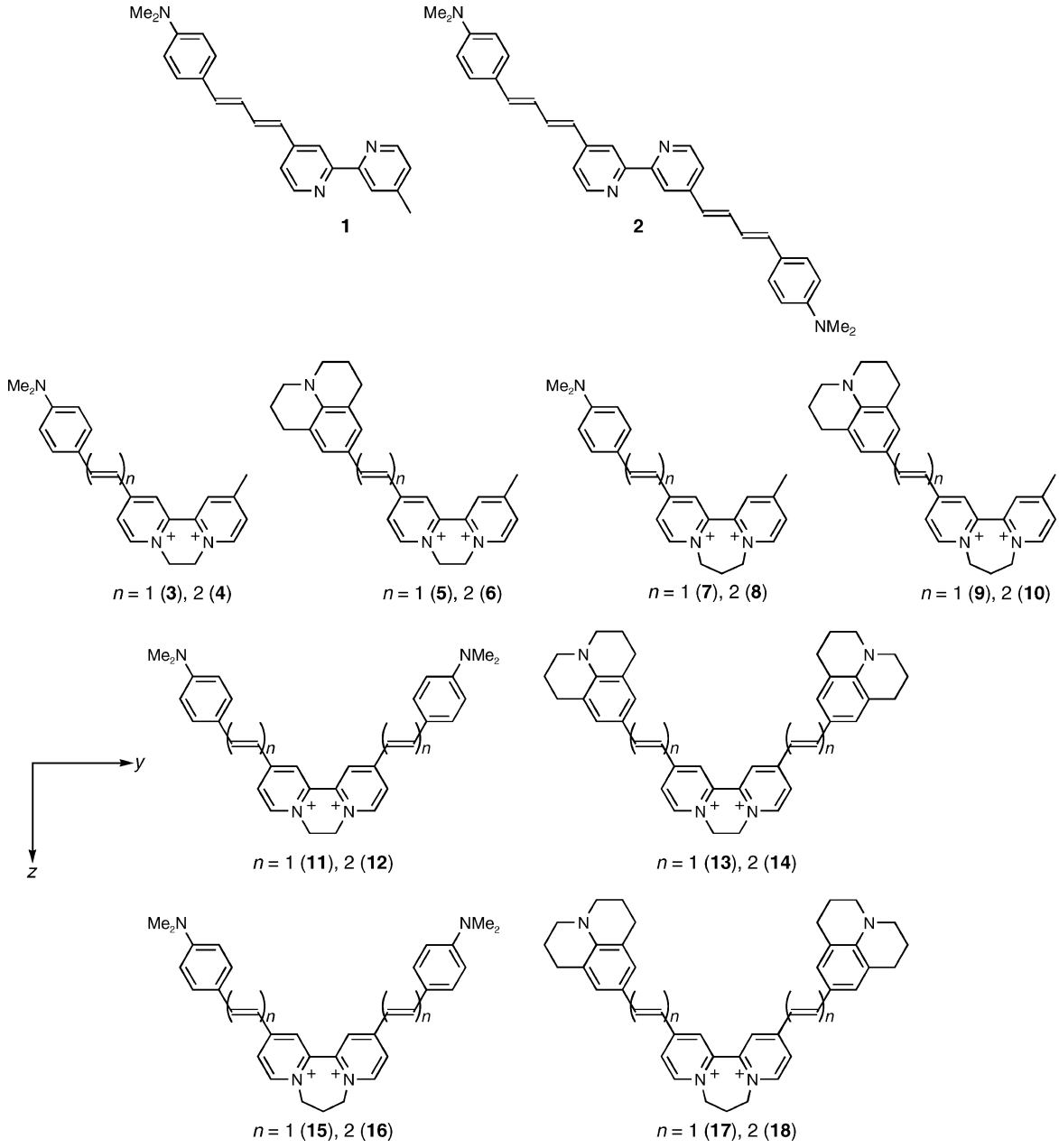

Figure 1. Chemical structures of the new diquat derivatives and precursors. Shorthand: EDQ^{2+} = ethylene diquat; PDQ^{2+} = propylene diquat. Except for some of the X-ray crystal structure determinations, all of the measurements on **3**−**18** were made with PF_6^- salts.

nizations followed our precedent set with EDQ^{2+} species,[17] designed to avoid the need for relatively forcing reaction conditions with dibromo precursors. The salts [**8**]$[PF_6]_2$ and [**16**]$[PF_6]_2$ were thus obtained pure in respective yields of 32 and 39%; these are lower than those reported previously[17] due to the poor solubility of **2** and the need for chromatography.

^{1}H NMR Spectroscopy Studies. The new compounds give diagnostic ^{1}H NMR spectra, and the signals for the protons of the diquat units show several noteworthy trends. Selected data are collected in Table 1 and representative spectra of salts [**7**]$[PF_6]_2$, [**9**]$[PF_6]_2$, [**13**]$[PF_6]_2$, and [**17**]$[PF_6]_2$ are shown in Figure S1 (Supporting Information) and Figure 2.

For the diquat aryl (C_5H_3N) protons, the low symmetry of the MS compounds generally leads to 6 resolved signals (4 doublets and 2 singlets), while the DS species show only 3 signals (2 doublets and 1 singlet) (Table 1). The diquat CH_2 protons afford a 4H singlet in the symmetrical DS EDQ^{2+} species. In all of the other compounds, the CH_2 protons give multiplets; two or three 2H signals for MS EDQ^{2+} and DS PDQ^{2+} species, respectively, but five signals (four 1H, one 2H) for MS PDQ^{2+} chromophores. Upfield shifts occur, up to 0.17 ppm in the C_5H_3N protons (Supporting Information, Figure S1), and up to 0.09 ppm in the diquat CH_2 protons, on replacing a 4-(dimethylamino)phenyl (Dap) group with julolidinyl (Jd). These shifts arise from greater shielding[18] caused by the stronger

(17) Coe, B. J.; Curati, N. R. M.; Fitzgerald, E. C. *Synthesis* **2006**, 146–150.

(18) Coe, B. J.; Foxon, S. P.; Harper, E. C.; Harris, J. A.; Helliwell, M.; Raftery, J.; Asselberghs, I.; Clays, K.; Franz, E.; Brunschwig, B. S.; Fitch, A. G. *Dyes Pigments* **2009**, *82*, 171–186.

Table 1. Selected ^{1}H NMR Data for the Salts [**3**−**18**][PF_6]$_2$[a]

dication	C_5H_3N signals						CH_2 signals				
3	8.70d	8.68s	8.58s	8.43d	8.07−8.01[b]	7.90d	4.98−4.93	4.84−4.80			
4	8.70d	8.68s	8.54s	8.45d	8.05d	7.96−7.89[b]	4.98−4.93	4.86−4.81			
5	8.69d	8.66s	8.46s	8.29d	8.05d	7.77d	4.98−4.92	4.80−4.74			
6	8.68d	8.66s	8.45s	8.35d	8.03d	7.80d	4.96−4.91	4.80−4.76			
7	8.74d	8.46d	8.20s	8.12s	8.09d	7.96−7.90[b]	4.80−4.74	4.64−4.58	4.40−4.32	4.16−4.08	2.75−2.67
8	8.74d	8.48d	8.19s	8.11−8.07		7.94d	4.80−4.74	4.65−4.58	4.38−4.30	4.17−4.08	2.75−2.67
9	8.73d	8.31d	8.18s	8.07d	7.98s	7.83−7.77[b]	4.80−4.72	4.58−4.49	4.42−4.30	4.11−3.98	2.79−2.60[c]
10	8.75d	8.40d	8.19s	8.08d	8.02s	7.86−7.78[b]	4.80−4.74	4.60−4.54	4.39−4.32	4.13−4.05	2.74−2.65[c]
11	8.63s	8.40d	7.89d				4.79s				
12	8.57s	8.43d	7.98−7.88[b]				4.80s				
13	8.46s	8.24d	7.73d				4.70s				
14	8.47s	8.31d	7.79d				4.74s				
15	8.45d	8.21s	7.99−7.91[b]				4.65−4.57	4.27−4.17	2.70−2.62		
16	8.47d	8.17s	7.92d				4.66−4.58	4.27−4.16	2.71−2.62		
17	8.30d	8.06s	7.77d				4.55−4.48	4.20−4.12	2.63−2.54		
18	8.36d	8.08s	7.94−7.85[b]				4.60−4.53	4.20−4.14	2.64−2.58		

[a] Recorded at 400 or 500 MHz in CD_3CN; all values are given in ppm with respect to TMS. [b] Overlapped with CH signals. [c] Overlapped with Jd CH_2 signals.

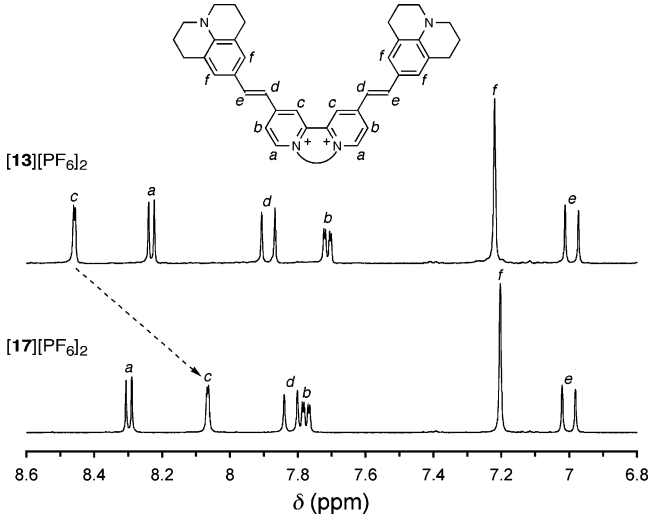

Figure 2. Aromatic regions of the ^{1}H NMR spectra of the salts [**13**][PF_6]$_2$ and [**17**][PF_6]$_2$ recorded at 400 MHz in CD_3CN at 293 K. The arrow indicates the largest shift observed for one of the C_5H_3N signals.

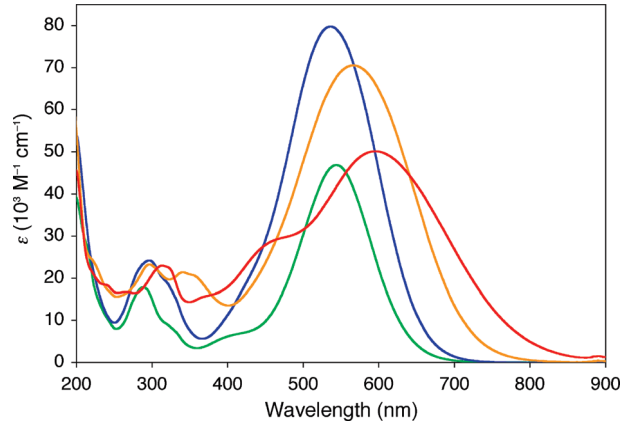

Figure 3. UV−vis absorption spectra of [**7**][PF_6]$_2$ (green), [**12**][PF_6]$_2$ (red), [**15**][PF_6]$_2$ (blue), and [**16**][PF_6]$_2$ (gold) at 293 K in acetonitrile.

π-ED ability of the Jd unit,[19] and are generally larger when $n = 1$ because the influence of the π-ED group(s) is communicated more strongly over shorter distances. Notably, increasing n also makes the chromophores more electron rich, but does not produce consistent effects on the chemical shifts of the diquat groups.

Large changes (up to 0.5 ppm) in the chemical shifts of the C_5H_3N signals occur on extending the diquaternized bridge (replacing EDQ^{2+} with PDQ^{2+}, Table 1). These environments are identified according to their splitting patterns, as confirmed via H,C-HMQC correlation studies with the model compounds [Me_2EDQ^{2+}][PF_6]$_2$ and [Me_2PDQ^{2+}][PF_6]$_2$. For the latter symmetric species, the largest difference is observed for the singlet (or finely split doublet) signal associated with the protons adjacent to the bridge between the two pyridyl rings (H^c); this signal shifts upfield from 8.63 ppm in [Me_2EDQ^{2+}][PF_6]$_2$ to 8.15 ppm in [Me_2PDQ^{2+}][PF_6]$_2$. In contrast, the other two signals (H^a and H^b) show smaller, accompanying downfield shifts of only 0.02−0.03 ppm. The fact that the signals for H^c and H^b are much closer together for [Me_2PDQ^{2+}][PF_6]$_2$ (at 8.15 and 8.12 ppm) indicates that these two environments become more similar as the diquat unit twists. The new substituted diquat derivatives show behavior similar to that of the model species (Figure 2).

Electronic Spectroscopy Studies. The UV−vis absorption data for salts [**3**−**18**][PF_6]$_2$ in acetonitrile are shown in Table 2, and representative spectra of [**7**][PF_6]$_2$, [**12**][PF_6]$_2$, [**15**][PF_6]$_2$, and [**16**][PF_6]$_2$ in Figure 3. All of the new compounds show intense absorptions in the visible region, attributable to Dap/Jd → diquat ICT transitions. For all of the EDQ^{2+} compounds, the main visible bands are accompanied by weaker features to high energy, while the PDQ^{2+} species show only one visible maximum. The less intense UV absorptions are due to $\pi \rightarrow \pi^*$ excitations that are expected to have lower directionality when compared with the ICT bands (i.e., processes largely confined within an aryl ring or ethenyl/butadienyl unit). It should be noted that the combination of relatively high energies and low intensities with small or neglible dipole-moment changes means that these excitations are not expected to contribute significantly to the NLO responses. The much lower ICT E_{max} values for [**3**][PF_6]$_2$ and [**7**][PF_6]$_2$ when compared with [DAS]PF_6[8a] confirm that the diquat units are considerably stronger π-EAs than a *N*-methylpyridinium group.[13]

The ICT energies E_{max} of the new chromophores show certain trends that are also observed with simpler pseudolinear mono-

(19) Kwon, O.; Barlow, S.; Odom, S. A.; Beverina, L.; Thompson, N. J.; Zojer, E.; Brédas, J.-L.; Marder, S. R. *J. Phys. Chem. A* **2005**, *109*, 9346–9352.

Table 2. UV−Vis Absorption and Electrochemical Data for Salts [**3**−**18**][PF_6]$_2$ and [DAS]PF_6 in Acetonitrile[a]

				E, V vs Ag-AgCl (ΔE_p, mV)[b]	
cation	λ_{max}, nm[a] (ε, 10^3 M^{-1} cm^{-1})	E_{max} (eV)	assignment	E_{pa}, oxidations	$E_{1/2}/E_{pc}$, reductions
3[c]	572 (38.0)	2.17	ICT	0.98	−0.41 (100)
	426 (12.7)	2.91	ICT		−0.82 (90)
	314 (22.7)	3.95	$\pi \rightarrow \pi^*$		
4	600 (39.4)	2.07	ICT	0.80	−0.41 (80)
	437 (13.5)	2.84	ICT		−0.80 (130)
	311 (20.4)	3.99	$\pi \rightarrow \pi^*$		
5	633 (39.2)	1.96	ICT	0.76	−0.47 (80)
	466 (11.2)	2.66	ICT		−0.86 (110)
	314 (18.0)	3.95	$\pi \rightarrow \pi^*$		
6	680 (42.6)	1.82	ICT	0.60	−0.43 (100)
	480 (12.9)	2.58	ICT		−0.84 (110)
	309 (20.3)	4.01	$\pi \rightarrow \pi^*$		
7	544 (46.9)	2.28	ICT	0.97	−0.61 (110)
	288 (17.9)	4.31	$\pi \rightarrow \pi^*$		−0.90 (100)
8	572 (43.8)	2.17	ICT	0.78	−0.58 (80)
	343 (10.1)	3.62	$\pi \rightarrow \pi^*$		−0.89 (70)
	286 (19.4)	4.34	$\pi \rightarrow \pi^*$		
9	602 (52.0)	2.06	ICT	0.77	−0.64 (110)
	286 (16.4)	4.34	$\pi \rightarrow \pi^*$		−0.91 (100)
10	644 (54.2)	1.93	ICT	0.62	−0.57 (120)
	376 (10.4)	3.30	$\pi \rightarrow \pi^*$		−0.89 (100)
	289 (17.8)	4.29	$\pi \rightarrow \pi^*$		
11[c]	560 (45.1)	2.21	ICT	0.98	−0.42 (90)
	442 (12.1)	2.81	ICT		−0.77 (80)
	318 (18.7)	3.90	$\pi \rightarrow \pi^*$		
12	596 (50.2)	2.08	ICT	0.78	−0.38 (80)
	460 (28.9)	2.70	ICT		−0.76 (120)
	313 (23.0)	3.96	$\pi \rightarrow \pi^*$		
13	615 (45.5)	2.02	ICT	0.76	−0.49 (100)
	477 (24.6)	2.60	ICT		−0.81 (125)
	317 (19.6)	3.91	$\pi \rightarrow \pi^*$		
14	669 (56.6)	1.85	ICT	0.60	−0.42 (80)
	507 (32.9)	2.45	ICT		−0.74 (160)
	316 (25.9)	3.92	$\pi \rightarrow \pi^*$		
15	535 (79.8)	2.32	ICT	0.97	−0.61 (80)
	297 (24.2)	4.18	$\pi \rightarrow \pi^*$		−0.88 (100)
16	566 (70.6)	2.19	ICT	0.79	−0.56 (100)
	341 (21.4)	3.64	$\pi \rightarrow \pi^*$		−0.82 (90)
	297 (23.2)	4.18	$\pi \rightarrow \pi^*$		
17	588 (82.5)	2.11	ICT	0.76	−0.65 (80)
	292 (20.3)	4.25	$\pi \rightarrow \pi^*$		−0.88 (80)
18	633 (71.3)	1.96	ICT	0.58	−0.58 (100)
	374 (18.3)	3.32	$\pi \rightarrow \pi^*$		−0.83 (80)
	298 (16.5)	4.16	$\pi \rightarrow \pi^*$		
DAS^{+d}	470 (42.8)	2.64	ICT	0.95[e]	−1.10[e]
	270 (11.1)	4.59	$\pi \rightarrow \pi^*$		

[a] Solutions ca. $2-3 \times 10^{-5}$ M. [b] Solutions ca. 10^{-3} M in analyte and 0.1 M in [$N(C_4H_9$-*n*$)_4$]PF_6 at a 2 mm disk glassy carbon working electrode with a scan rate of 200 mV s^{-1}. Ferrocene internal reference $E_{1/2} = 0.46$ V, $\Delta E_p = 80-100$ mV. [c] Data taken from ref 13. [d] Data taken from refs 8a and 8c. [e] Conditions as for other compounds, but using a 2 mm Pt disk working electrode.

cations.[18] Thus, in keeping with the ^{1}H NMR data (see above), replacing Dap with the stronger π-ED Jd decreases E_{max} by 0.19−0.26 eV, while moving from $n = 1$ to 2 gives smaller decreases of 0.07−0.17 eV (Table 2, Figure 3). In contrast, moving from an EDQ^{2+} chromophore to its PDQ^{2+} analogue causes blue shifts in the ICT bands (Figure 3); when considering only the dominant low energy bands for the EDQ^{2+} species, the increase in E_{max} is almost constant at ca. 0.1 eV. This trend is consistent with the lower relative π-EA strength of a PDQ^{2+} unit, noted in previous electrochemical studies[20] (and see below). Often small but significant changes in E_{max} are also found on moving from a MS chromophore to its DS counterpart (Figure 3). For the EDQ^{2+} species, E_{max} of the dominant band increases by 0.01−0.06 eV, while the accompanying higher energy band shifts to lower energy by 0.06−0.14 eV. For the PDQ^{2+} chromophores, the energies of the single ICT bands increase by 0.02−0.05 eV as a result of this structural change.

Trends are also observed in the molar extinction coefficients ε of the ICT bands. Moving from $n = 1$ to 2 increases ε (but not always greatly) for all the EDQ^{2+} species, whereas the opposite occurs for the PDQ^{2+} chromophores (Figure 3), except the pair [**9**/**10**][PF_6]$_2$. In our previous studies,[18] replacing Dap with Jd always increased ε; the same is generally observed for [**3**−**18**][PF_6]$_2$, excepting the minor, high energy ICT bands of the pairs [**3**/**5**][PF_6]$_2$ and [**4**/**6**][PF_6]$_2$. However, these intensity increases are generally only quite small. Moving from an EDQ^{2+} chromophore to its PDQ^{2+} analogue always increases ε substantially (Figure 3); with regards to NLO properties, it may be anticipated that this effect will compensate for the relatively higher E_{max} values of the PDQ^{2+} species (see below). The ε

(20) Kuzuya, M.; Kondo, S.-I.; Murase, K. *J. Phys. Chem.* **1993**, *97*, 7800–7802.

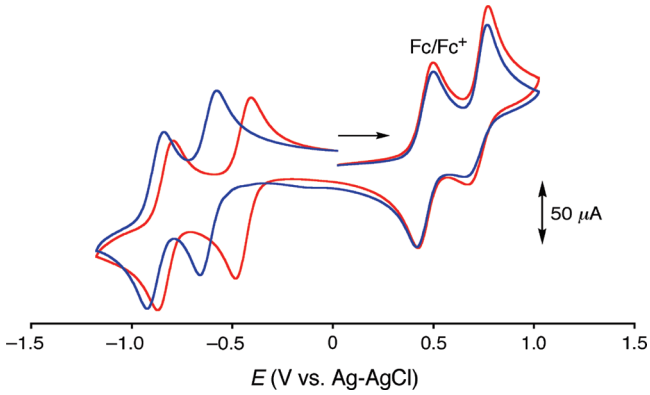

Figure 4. Cyclic voltammograms for the salts $[\mathbf{5}][PF_6]_2$ (red) and $[\mathbf{9}][PF_6]_2$ (blue) recorded at 200 mV s^{-1} in acetonitrile with a glassy carbon working electrode (Fc = ferrocene internal standard). The arrow indicates the direction of the initial scans.

values for the DS species are always rather larger than those of their MS counterparts (Figure 3), except for the minor ICT band for the pair $[\mathbf{3}/\mathbf{11}][PF_6]_2$.

Electrochemical Studies. Cyclic voltammetric data for salts $[\mathbf{3}-\mathbf{18}][PF_6]_2$ in acetonitrile are shown in Table 2, and representative voltammograms of $[\mathbf{5}][PF_6]_2$ and $[\mathbf{9}][PF_6]_2$ in Figure 4. Although they are always irreversible, the E_{pa} values ascribed to oxidation of the Dap/Jd units display trends that are also found with related monocations,[18] and are consistent with the ^{1}H NMR and ICT data (see above). Moving from $n = 1$ to 2 causes E_{pa} to decrease by 150−200 mV, while similar changes of 160−230 mV are observed on replacing Dap with Jd. Oxidation hence becomes easier as both structural modifications make the molecules more electron rich. In contrast, moving from an EDQ^{2+} chromophore to its PDQ^{2+} analogue or from a MS compound to its DS counterpart leaves the E_{pa} values almost or completely unchanged.

The salt $[DAS]PF_6$ shows only one, irreversible reduction wave at relatively low potential,[8a] consistent with the moderate π-EA strength of a single pyridinium ring (Table 2). The reductive electrochemical behavior of the diquat units in $[\mathbf{3}-\mathbf{18}][PF_6]_2$ is more interesting, with each compound showing two reversible or quasireversible one-electron waves. Moving from $n = 1$ to 2 causes the $E_{1/2}$ values to increase slightly by up to 70 mV (and the shifts are generally largest for the first wave), whereas moving from a MS compound to its DS analogue has little effect on the first $E_{1/2}$ value but increases the second by up to 100 mV. The reduction processes thus become easier, and these changes can be attributed to more effective delocalization of the extra electron(s) in the reduced forms due to extension of the π-conjugated systems. Replacing Dap with Jd either barely affects the $E_{1/2}$ values or produces small decreases of up to 70 mV because the presence of the stronger π-ED group(s) makes reduction more difficult. The lower π-EA strength of a PDQ^{2+} as opposed to a EDQ^{2+} unit, noted in previous electrochemical studies[20] (and evidenced by the ICT energies) leads to relatively large decreases in the $E_{1/2}$ values (Figure 4). For the first wave, shifts of 140−200 mV are observed, while the second wave shows smaller changes of 50−110 mV. The main cause of this weaker relative π-EA ability is the propylene bridging unit that prevents the pyridyl rings from becoming coplanar and thus hinders effective delocalization of the extra electron(s) in the reduced species.

X-ray Crystallography. While this study concerns primarily molecular properties, bulk NLO behavior is required for potential applications, and for quadratic effects polar structures are essential. We have obtained single-crystal X-ray structures for nine salts of our new chromophores. Six of these (with data 99% complete to 20.82° or better) are presented here, with crystallographic data and refinement details in Table 3, while the others are included in the CIF provided as Supporting Information. Eight of the structures contain PDQ^{2+}-based chromophores, which seem to crystallize better than their EDQ^{2+} counterparts, perhaps due to more efficient packing that allows the formation of larger crystals.

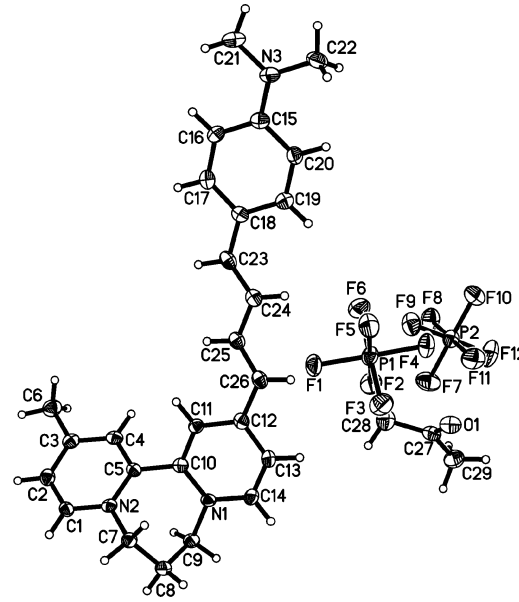

Figure 5. Representation of the molecular structure of $[\mathbf{8}][PF_6]_2 \cdot Me_2CO$ (50% probability ellipsoids).

The salt $[\mathbf{8}][PF_6]_2 \cdot Me_2CO$ (Figure 5) forms large crystals and provides the highest quality structure achieved in this study. The dihedral angle (Table 4) between the planes of the two pyridyl rings is slightly lower than those in published structures of PDQ^{2+} units (51.4 and 59.7°).[21] Other geometric parameters are unremarkable (Table S1, Supporting Information), as for all the other structures. The **8** dications pack in layers parallel to the crystallographic *ab* plane. Although the packing within each layer is polar, the layers oppose each other so that the overall structure is centrosymmetric. In the salt $[\mathbf{13}][OTf]_2 \cdot 2MeCN$ (Figure 6), the py/py angle (Table 4) is much lower than that in $[\mathbf{8}][PF_6]_2 \cdot Me_2CO$, but slightly above the range of 15−24° found in comparable published structures.[22] The **13** dications form polar chains parallel to the crystallographic *b* axis; these chains align antiparallel, giving a centrosymmetric structure.

The structure of $[\mathbf{15}][NapSO_3]_2 \cdot 2H_2O$ (Figure 7a) is especially notable, as its noncentrosymmetric *Aba*2 space group and polar packing (Figure 7b) mean that this material will show bulk NLO activity. This structure contains H-bonded chains of $NapSO_3^-$ anions and water molecules parallel to the crystallographic *c* axis. The H-bond distances between the water oxygen O1W and the $NapSO_3^-$ oxygens O3 and O2 are 2.751(14) Å and 2.957(16) Å, respectively. The V-shaped cations form chains along the *c* axis, all with the same polar

(21) (a) Mori, Y.; Matsuyama, Y.; Yamada, S.; Maeda, K. *Acta Crystallogr., Sect. C* **1992**, *48*, 894–897. (b) Knoch, F.; Smauch, G.; Kisch, H. *Z. Kristallogr.* **1995**, *210*, 225.

(22) Cambridge Structural Database, Version 5.30, May 2009 (update).

Table 3. Crystallographic Data and Refinement Details for the Salts [**8**][PF_6]$_2$·Me_2CO, [**13**][OTf]$_2$·2MeCN, [**15**][$NapSO_3$]$_2$·$2H_2O$, [**16**][$NapSO_3$]$_2$·$2H_2O$, [**17**][PF_6]$_2$·2MeCN, and [**18**][PF_6]$_2$·$2Me_2CO$

	[**8**][PF_6]$_2$·Me_2CO	[**13**][OTf]$_2$·2MeCN	[**15**][$NapSO_3$]$_2$·$2H_2O$	[**16**][$NapSO_3$]$_2$·$2H_2O$	[**17**][PF_6]$_2$·2MeCN	[**18**][PF_6]$_2$·$2Me_2CO$
formula	$C_{29}H_{35}F_{12}N_3OP_2$	$C_{46}H_{48}F_6N_6O_6S_2$	$C_{53}H_{54}N_4O_8S_2$	$C_{57}H_{58}N_4O_8S_2$	$C_{45}H_{50}F_{12}N_6P_2$	$C_{51}H_{60}F_{12}N_4O_2P_2$
M	731.54	959.02	939.12	991.19	964.85	1050.97
crystal system	triclinic	monoclinic	orthorhombic	orthorhombic	monoclinic	monoclinic
space group	$P\bar{1}$	$C2/c$	$Aba2$	$Pbcn$	$C2/c$	$C2/c$
a, Å	8.3822(4)	18.315(2)	10.310(4)	10.055(5)	19.870(5)	33.971(3)
b, Å	11.8966(6)	16.102(1)	35.92(1)	12.875(7)	15.248(5)	8.5208(9)
c, Å	16.7255(8)	15.462(1)	12.402(5)	37.90(2)	15.184(5)	20.299(2)
α, deg	97.812(4)	90	90	90	90	90
β, deg	99.103(4)	103.33(1)	90	90	106.185(5)	124.043(1)
γ, deg	104.236(4)	90	90	90	90	90
V, Å^3	1569.42(13)	4437.0(7)	4592(3)	4906(4)	4418(2)	4868.8(8)
Z	2	4	4	4	4	4
T, K	100(2)	100(2)	100(2)	100(2)	100(2)	100(2)
μ, mm^{-1}	0.240	0.202	0.178	0.171	0.191	0.181
crystal size, mm^3	0.35 × 0.18 × 0.15	0.50 × 0.35 × 0.20	0.50 × 0.30 × 0.05	0.50 × 0.30 × 0.05	0.40 × 0.10 × 0.06	0.13 × 0.05 × 0.01
crystal appearance	dark purple block	dark blue block	red plate	brown rod	black needle	dark blue plate
reflections collected	15497	6696	11761	25106	15664	18357
independent reflections (R_{int})	6397 (0.0371)	2297 (0.0536)	2794 (0.1155)	3491 (0.1821)	3891 (0.1148)	4436
θ_{max}, deg (completeness)	26.37 (99.7%)	20.82 (99%)	21.97 (99.9%)	23.26 (99%)	25.03 (99.8%)	25.35 (99.4%)
reflections with $I > 2\sigma(I)$	3787	1462	2154	2578	2421	3261
parameters	429	331	274	459	297	323
goodness-of-fit on F^2	0.947	1.270	1.091	1.131	1.107	1.023
final R1, wR2 [$I > 2\sigma(I)$][a]	0.0405, 0.0930	0.1053, 0.2963	0.0995, 0.2342	0.1143, 0.2491	0.1026, 0.2071	0.0447, 0.1208
(all data)	0.0758, 0.1064	0.1431, 0.3305	0.1239, 0.2494	0.1370, 0.2598	0.1554, 0.2315	0.0677, 0.1090
Flack parameter	N/A	N/A	0.3(3)[b]	N/A	N/A	N/A
peak and hole (e·Å^{-3})	0.370, −0.365	0.573, −0.352	0.513, −0.277	0.301, −0.274	0.802, −0.357	0.567, −0.291

[a] The structures were refined on F_o^2 using all data; the values of R1 are given for comparison with older refinements based on F_o with a typical threshold of $F_o > 4\sigma(F_o)$. [b] Two data sets were obtained, but neither was strong enough to allow accurate determination of the absolute structure given the absence of any atoms heavier than sulfur.

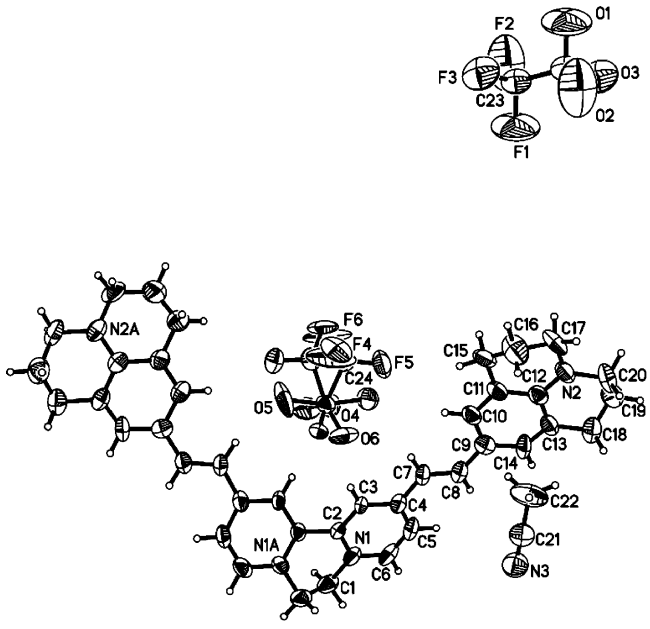

Figure 6. Representation of the molecular structure of [**13**][OTf]$_2$·2MeCN, showing only the single acetonitrile molecule in the asymmetric unit (30% probability ellipsoids).

orientation, separated by layers of anions. X-ray powder diffraction (Supporting Information, Figure S2) confirms that this material can be obtained in substantial quantities, offering potential for bulk NLO measurements.

In contrast to [**15**][$NapSO_3$]$_2$·$2H_2O$, [**16**][$NapSO_3$]$_2$·$2H_2O$ (Figure 8a) forms a centrosymmetric structure. Although both structures contain $NapSO_3^-$···H_2O H-bonded chains, [**16**][$NapSO_3$]$_2$·$2H_2O$ has alternating chains of dications aligned

Table 4. Selected Twist Angles (deg) for the Diquat Salts

salt	py/py[a]	bridge/py[b]	bridge/Ph[c]
[**8**][PF_6]$_2$·Me_2CO	48.6	8.5	3.8
[**13**][OTf]$_2$·2MeCN	27.3	2.8	5.3
[**15**][$NapSO_3$]$_2$·$2H_2O$	57.4	9.5	14.1
[**16**][$NapSO_3$]$_2$·$2H_2O$	58.9	6.6	20.0
[**17**][PF_6]$_2$·2MeCN	49.0	1.0	6.4
[**18**][PF_6]$_2$·$2Me_2CO$	46.6	13.0	2.8

[a] Dihedral angle between the planes of the two pyridyl rings. [b] Torsion angle between the ethenyl/butadienyl unit and the attached pyridyl ring. [c] Torsion angle between the ethenyl/butadienyl unit and the attached phenyl ring.

antiparallel (Figure 8b). The H-bonds in [**16**][$NapSO_3$]$_2$·$2H_2O$ occur between the water O1W positions and disordered oxygens on the $NapSO_3^-$ anion, with D···A distances of 2.69(1), 2.79(1), 2.80(2), and 2.94(2) Å to O3, O1, O2B, and O3B, respectively. Clearly, the increase in cation size induces substantial changes in the packing arrangement. However, the salts [**17**][PF_6]$_2$·2MeCN (Supporting Information, Figure S3) and [**18**][PF_6]$_2$·$2Me_2CO$ (Supporting Information, Figure S4) adopt very similar packing structures, with the dications in antiparallel-aligned polar chains parallel to the crystallographic b axis. The lower resolution structures of [**7**][$NapSO_3$]$_2$, [**7**][PF_6]$_2$·MeCN and [**9**][PF_6]$_2$·MeCN are included in the Supporting Information (Figures S5−S7 and CIF).

Hyper-Rayleigh Scattering Studies. The β values of salts [**3**−**18**][PF_6]$_2$ measured in acetonitrile by using the HRS technique[23,24] with a 800 nm Ti^{3+}:sapphire laser are shown in Table 5. This wavelength was chosen because the ICT bands

(23) (a) Clays, K.; Persoons, A. *Phys. Rev. Lett.* **1991**, *66*, 2980–2983. (b) Clays, K.; Persoons, A. *Rev. Sci. Instrum.* **1992**, *63*, 3285–3289. (c) Hendrickx, E.; Clays, K.; Persoons, A. *Acc. Chem. Res.* **1998**, *31*, 675–683.

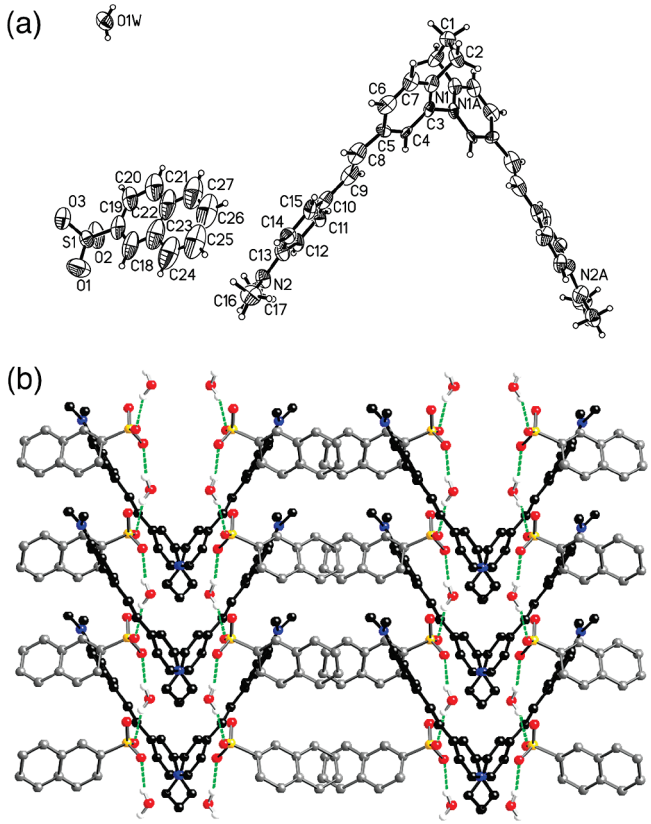

Figure 7. Representations of the structure of [**15**][$NapSO_3$]$_2$·2H_2O. (a) Molecular structure (50% probability ellipsoids); the cation has been completed by generating symmetry equivalent atoms, but only the single $NapSO_3^-$ anion and water molecule in the asymmetric unit are shown. (b) Crystal packing and H-bonding, viewed along the crystallographic *a* axis; cation C = black; other C = gray; N = blue; O = red; S = yellow (H atoms omitted except for the crystallographically located water atoms; H-bonds are shown as green lines).

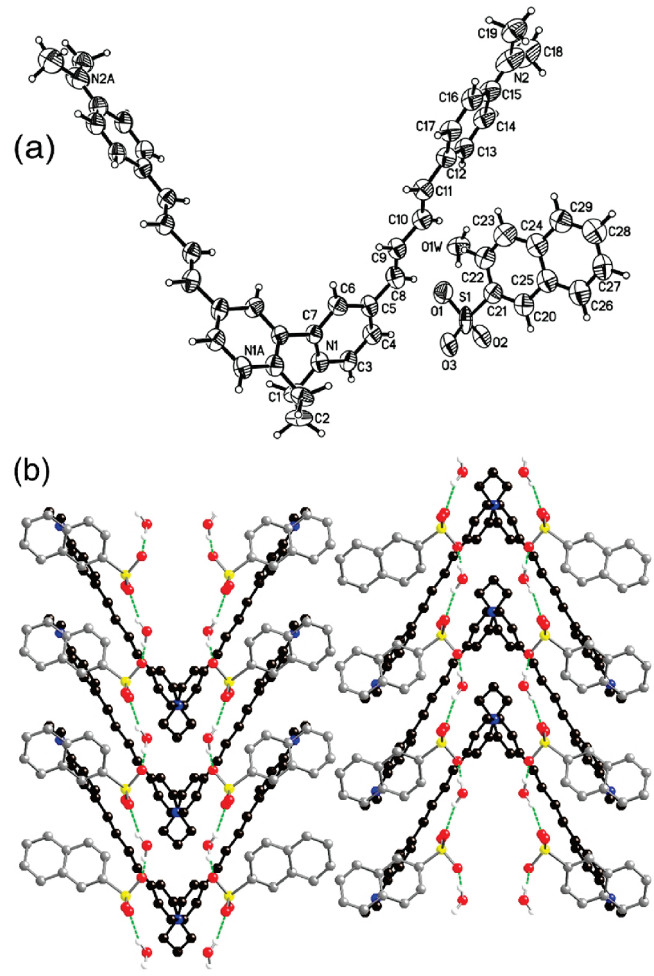

Figure 8. Representations of the structure of [**16**][$NapSO_3$]$_2$·2H_2O. (a) Molecular structure, with the disorder of the $NapSO_3^-$ anions removed (50% probability ellipsoids). (b) Crystal packing and H-bonding. All other details are as for Figure 7.

lie between 800 nm and the second harmonic (SH) at 400 nm (Figure 3). However, the compounds do absorb relatively strongly at 400 nm, and also at 800 nm for most of the Jd species, and thus the results obtained are generally markedly resonance enhanced. Other available lasers, e.g., 1064 or 1300 nm, would be unsuitable for most of the samples due to very strong absorption at their SH wavelengths. The data shown are orientationally averaged $\sqrt{\langle\beta_{HRS}^2\rangle}$ values derived from the total HRS intensity, regardless of molecular symmetry.

Although many of the chromophores show an additional ICT maximum to high energy of the main band and there is significant resonance enhancement, we have used the simple two-state model[25] and the major λ_{max} values (Table 2) to estimate β_0 values (Table 5). It should be noted that this analysis constitutes a major oversimplification because the diquat derivatives, especially the DS ones, cannot be accurately described as two-state systems, as confirmed by the theoretical studies that reveal multiple low-energy excited states (see below). Nevertheless, it is notable that all of the chromophores do display one dominant visible maximum (and *only* one for the PDQ^{2+} species), and most of the derived β_0 values are larger than that determined under the same conditions for [DAS]PF_6,[8b,c] and in several cases ca. 2−3-fold increased when compared with this benchmark. As also observed with related 1D species,[18] β_0 increases substantially either when moving from $n = 1$ to 2 (except for the pair [**9**/**10**][PF_6]$_2$), or on replacing Dap with Jd (excepting the pair [**8**/**10**][PF_6]$_2$). While moving from a EDQ^{2+} chromophore to its PDQ^{2+} analogue apparently causes β_0 to decrease, this is not always the case. Likewise, the β_0 responses of the DS compounds are mostly larger than for their MS counterparts, but several exceptions to this trend are found. Given the caveats mentioned above and since these comments also relate to the β_0 values determined without considering molecular symmetry differences, they should be viewed with caution.

The electronic structures and thus hyperpolarizabilities of these chromophores are in fact substantially 2D in nature, and the main value of our HRS measurements is not actually to estimate β_0 values, but rather to probe the relative importance of different tensor components. A chromophore with C_{2v} symmetry has five nonzero components of the β tensor, β_{zzz}, β_{zyy}, β_{zxx}, β_{yyz}, and β_{xxz}. Assuming Kleinman symmetry, $\beta_{zyy} = \beta_{yyz}$ and $\beta_{zxx} = \beta_{xxz}$, and if the structure is essentially 2D, then

(24) (a) Olbrechts, G.; Strobbe, R.; Clays, K.; Persoons, A. *Rev. Sci. Instrum.* **1998**, *69*, 2233–2241. (b) Olbrechts, G.; Wostyn, K.; Clays, K.; Persoons, A. *Opt. Lett.* **1999**, *24*, 403–405. (c) Clays, K.; Wostyn, K.; Olbrechts, G.; Persoons, A.; Watanabe, A.; Nogi, K.; Duan, X.-M.; Okada, S.; Oikawa, H.; Nakanishi, H.; Vogel, H.; Beljonne, D.; Brédas, J.-L. *J. Opt. Soc. Am. B* **2000**, *17*, 256–265. (d) Franz, E.; Harper, E. C.; Coe, B. J.; Zahradnik, P.; Clays, K.; Asselberghs, I. *Proc. SPIE-Int. Soc. Opt. Eng* **2008**, *6999*, 699923-1–699923-11.
(25) (a) Oudar, J. L.; Chemla, D. S. *J. Chem. Phys.* **1977**, *66*, 2664–2668. (b) Oudar, J. L. *J. Chem. Phys.* **1977**, *67*, 446–457.

Table 5. HRS Data and Depolarization Ratios for Salts [**3**−**18**][PF_6]$_2$ and [DAS]PF_6 in Acetonitrile

cation	$\sqrt{\langle\beta^2_{HRS}\rangle}$[a] ($10^{-30}$ esu)	β_0[b] (10^{-30} esu)	ρ[c]	k	β_{zzz}[d] (10^{-30} esu)	β_{zyy}[d] (10^{-30} esu)
3	115 ± 50	58 ± 29	2.9 ± 0.4		277 ± 120	
4	272 ± 9	148 ± 5	3.0 ± 0.5		655 ± 22	
5	414 ± 25	233 ± 14	3.5 ± 0.5		1000 ± 60	
6	498 ± 43	261 ± 23	4.1 ± 0.6		1200 ± 100	
7	128 ± 12	58 ± 5	3.4 ± 0.5		310 ± 30	
8	255 ± 25	130 ± 12	3.6 ± 0.5		615 ± 60	
9	263 ± 22	144 ± 12	3.3 ± 0.5		630 ± 55	
10	224 ± 16	126 ± 9	3.3 ± 0.5		540 ± 40	
11	140 ± 58	68 ± 28	2.7 ± 0.4	9	25 ± 10	230 ± 100
12	300 ± 18	163 ± 10	3.2 ± 0.5	3	150 ± 25	460 ± 75
13	321 ± 97	179 ± 54	2.5 ± 0.4	10	50 ± 15	520 ± 175
14	473 ± 86	256 ± 46	2.7 ± 0.4	9	85 ± 20	770 ± 180
15	212 ± 20	92 ± 9	2.9 ± 0.4	5	70 ± 10	335 ± 60
16	276 ± 25	138 ± 13	3.4 ± 0.5	3	140 ± 25	420 ± 75
17	190 ± 15	101 ± 8	2.7 ± 0.4	9	35 ± 6	310 ± 50
18	603 ± 32	339 ± 18	2.3 ± 0.3	10	100 ± 15	980 ± 150
DAS^{+e}	440 ± 30	110 ± 7				

[a] Orientationally averaged β without any assumption of symmetry or contributing tensor elements, measured by using an 800 nm Ti^{3+}:sapphire laser. The quoted cgs units (esu) can be converted into SI units ($C^3\ m^3\ J^{-2}$) by dividing by a factor of 2.693×10^{20}. [b] Static β estimated from $\sqrt{\langle\beta^2_{HRS}\rangle}$ via the two-state model.[25] Note that the uncertainties quoted are merely statistical and do not account for any errors introduced by two-state extrapolation. [c] Depolarization ratio. [d] β tensor components derived from the HRS intensity and ρ. [e] Data taken from refs 8b and c.

$\beta_{zxx} = \beta_{xxz} = 0$, so only β_{zzz} and β_{zyy} are significant. These DS diquat derivatives have a somewhat distorted C_{2v} geometry that retains C_2 symmetry. The calculated tensor components are nevertheless analogous to those of C_{2v} molecules, being dominated by the β_{zzz} and β_{zyy} terms. In order to assess the importance of "off-diagonal" tensor components, we have measured HRS depolarization ratios ρ for salts [**3**−**18**][PF_6]$_2$ and these are included in Table 5. The parameter ρ is the ratio of the intensities of the scattered SH light polarized parallel and perpendicular to the polarization direction of the fundamental beam.[26] A ρ value of 5 is the upper limit for purely dipolar symmetry, corresponding with a single dipolar β_{zzz} tensor component, and under ideal experimental conditions. Realistic experimental conditions, such as the use of a condenser system to collect the SH light, will induce a lowering of the observed ρ value. The octupolar reference compound crystal violet gives a ρ value of 1.5.

Treatment of our experimental data (for the method, see the Supporting Information) affords the β_{zzz} and β_{zyy} values shown in Table 5. All of the MS compounds [**3**−**10**][PF_6]$_2$ exhibit a ρ value of at least 2.9, and up to 4.1, with an average of 3.4 ± 0.3 clearly confirming the dominance of a single β_{zzz} tensor component. The DS chromophores in [**11**−**18**][PF_6]$_2$ show ρ values between 2.3 and 3.4, with an average of 2.8 ± 0.3, significantly lower than for their MS counterparts. Because the MS species are predominantly 1D dipoles, we have not attempted to derive their β_{zyy} values, but the shapes of the DS species do justify such analyses. In each case, β_{zyy} dominates markedly over β_{zzz} (Table 5). Given that the two types of chromophore have been treated differently, assuming purely 1D dipolar symmetry ($C_{\infty v}$) for the MS species but simplified C_{2v} symmetry for the DS derivatives, comparing the β_{zzz} values for MS/DS pairs is inappropriate. However, for the DS species, both β_{zzz} and β_{zyy} generally increase significantly when moving from $n = 1$ to 2. Although these tensor components show no clear dependence on the nature of the π-ED or diquat units, k (i.e., β_{zyy}/β_{zzz}) always increases on replacing Dap with Jd.

(26) Heesink, G. J. T.; Ruiter, A. G. T.; van Hulst, N. F.; Bölger, B. *Phys. Rev. Lett.* **1993**, *71*, 999–1002.

Stark Spectroscopic Studies. Stark spectroscopy[27] affords dipole-moment changes that can be used with other parameters to estimate β_0 values via the two-state model.[25] Data obtained for salts [**3**−**18**][PF_6]$_2$ in butyronitrile at 77 K are shown in Table 6, and representative spectra for [**9**][PF_6]$_2$, [**10**][PF_6]$_2$ and [**18**][PF_6]$_2$ are shown in Figure 9.

The ICT bands of [**3**−**18**][PF_6]$_2$ generally show slight blue shifts on moving from acetonitrile solutions to butyronitrile glasses (Tables 2 and 6). All of the trends in E_{max} noted at room temperature are maintained at 77 K. The band intensities at 77 K, quantified by f_{os} and μ_{12} (summed for [**11**−**18**][PF_6]$_2$) show trends that mostly agree with those already noted for the ε values (see above). Moving from $n = 1$ to 2 always increases μ_{12}, while f_{os} generally increases only for the EDQ^{2+} species. Replacing Dap with Jd gives broadly similar behavior. In every case, either replacing EDQ^{2+} with PDQ^{2+} or moving from a MS to its DS counterpart increases f_{os} and μ_{12}, and the latter structural change always gives by far the largest increases in absorption intensity.

The dipole-moment changes and electron-transfer distances ($\Delta\mu_{12}$, $\Delta\mu_{ab}$, r_{12}, and r_{ab}; averaged for [**11**−**18**][PF_6]$_2$) logically always increase with molecular length on moving from $n = 1$ to 2 (Table 6). However, swapping Dap for Jd gives no clear trends for these parameters. In most cases, replacing EDQ^{2+} with PDQ^{2+} gives small decreases in $\Delta\mu_{12}$, $\Delta\mu_{ab}$, r_{12}, and r_{ab}, while moving from a MS to the related DS dication slightly increases these parameters. The terms c_b^2 and H_{ab} (again, averaged for [**11**−**18**][PF_6]$_2$) quantify π-ED-EA coupling and orbital mixing and always decrease, or show no significant change, on moving from $n = 1$ to 2. These observations are consistent with the ^1H NMR studies (see above), and predictable because π-orbital overlap weakens over longer distances. Generally, c_b^2 and H_{ab} also decrease on moving from a MS chromophore to its DS analogue. Replacing Dap with Jd does not generally change c_b^2 or H_{ab} significantly. Comparing EDQ^{2+} and PDQ^{2+} pairs reveals similar c_b^2 values, but significantly higher H_{ab} values for the EDQ^{2+} species.

(27) (a) Liptay, W. In *Excited States*; Lim, E. C., Ed.; Academic Press, New York, 1974, Vol. 1, pp 129−229. (b) Bublitz, G. U.; Boxer, S. G. *Annu. Rev. Phys. Chem.* **1997**, *48*, 213–242. (c) Vance, F. W.; Williams, R. D.; Hupp, J. T. *Int. Rev. Phys. Chem.* **1998**, *17*, 307–329. (d) Brunschwig, B. S.; Creutz, C.; Sutin, N. *Coord. Chem. Rev.* **1998**, *177*, 61–79.

Table 6. ICT Absorption and Stark Spectroscopic Data for Salts [**3**−**18**][PF_6]$_2$ and [DAS]PF_6

cation	ν_{max}[a] (cm^{-1})	λ_{max}[a] (nm)	E_{max}[a] (eV)	f_{os}[b]	μ_{12}[c] (D)	$\Delta\mu_{12}$[d] (D)	$\Delta\mu_{ab}$[e] (D)	r_{12}[f] (Å)	r_{ab}[g] (Å)	c_b^2[h]	H_{ab}[i] (10^3 cm^{-1})	β_0[j] (10^{-30} esu)	$\Sigma\beta_0$ (10^{-30} esu)
3[k]	17762	563	2.20	0.50	7.7	20.6	25.8	4.3	5.4	0.10	5.3	297	
4	16779	596	2.08	0.51	8.0	26.4	31.0	5.5	6.5	0.07	4.3	456	
5	16212	617	2.01	0.57	8.6	20.5	26.8	4.3	5.6	0.12	5.2	439	
6	15244	656	1.89	0.63	9.4	26.6	32.9	5.5	6.9	0.09	4.4	778	
7	18631	537	2.31	0.66	8.7	18.1	25.3	3.8	5.3	0.13	6.5	305	
8	17421	574	2.16	0.73	9.5	24.7	31.1	5.1	6.5	0.10	5.3	525	
9	17099	585	2.12	0.65	9.0	17.5	25.3	3.6	5.3	0.15	6.1	372	
10	16050	623	1.99	0.74	9.9	24.4	31.5	5.1	6.6	0.11	5.1	705	
11[k]	17911 (17730)	558 (564)	2.22 (2.20)	1.00	11.0	23.6	32.2	4.9	6.7	0.13	6.0	688	876
	22518 (22883)	444 (437)	2.79 (2.84)	0.54	7.1	25.7	29.4	5.6	6.1	0.06	5.5	188	
12	16857 (15728)	593 (636)	2.09 (1.95)	0.37	7.1	30.0	33.1	6.2	6.9	0.05	3.4	462	1173
	(17502)	(571)	(2.17)	0.49	7.7	30.1	33.8	6.3	7.0	0.05	4.0	445	
	21212 (21454)	471 (466)	2.63 (2.66)	0.48	6.9	34.0	36.7	7.1	7.6	0.04	4.0	266	
13	16615 (14437)	602 (693)	2.06 (1.79)	0.07	3.3	16.0	17.3	3.3	3.6	0.04	2.7	63	905
	(16494)	(607)	(2.05)	0.92	10.9	20.4	29.9	4.3	6.2	0.16	6.0	679	
	20890 (21172)	478 (472)	2.59 (2.63)	0.40	6.4	23.6	26.8	4.9	5.6	0.06	5.0	163	
14	15486 (14126)	646 (708)	1.92 (1.75)	0.31	6.9	27.6	30.9	5.8	6.4	0.05	3.1	500	1500
	(15888)	(629)	(1.97)	0.60	8.9	30.2	35.1	6.3	7.3	0.07	4.0	725	
	19455 (19757)	514 (506)	2.41 (2.45)	0.41	6.6	32.3	34.9	6.7	7.3	0.04	3.8	275	
15	18954 (17825)	528 (561)	2.35 (2.21)	0.20	5.1	19.2	21.8	4.0	4.5	0.06	4.2	119	738
	(19196)	(521)	(2.38)	1.10	10.9	20.5	29.9	4.3	6.2	0.16	7.0	498	
	(22584)	(443)	(2.80)	0.40	5.9	23.2	26.1	4.8	5.4	0.05	5.1	121	
16	17664 (16615)	566 (602)	2.19 (2.06)	0.34	6.6	24.0	27.4	5.0	5.7	0.06	4.0	289	1126
	(18147)	(551)	(2.25)	0.86	10.1	26.3	33.1	5.5	6.9	0.10	5.5	617	
	(20608)	(485)	(2.56)	0.48	7.0	24.9	28.6	5.2	6.0	0.06	5.1	220	
17	17422 (16091)	574 (622)	2.16 (2.00)	0.11	3.7	19.6	21.0	4.1	4.4	0.03	2.8	79	943
	(17462)	(573)	(2.17)	1.09	11.5	21.5	31.5	4.5	6.6	0.16	6.4	712	
	(20648)	(484)	(2.56)	0.33	5.8	24.9	27.5	5.2	5.7	0.05	4.4	152	
18	16292 (15244)	614 (656)	2.02 (1.89)	0.28	6.2	23.6	26.7	5.8	6.4	0.05	3.5	297	1390
	(16615)	(602)	(2.06)	0.80	10.1	27.4	34.1	6.1	6.7	0.10	4.9	770	
	(18873)	(530)	(2.34)	0.53	7.7	25.5	29.8	6.9	7.3	0.07	4.9	323	
DAS^+[l]	20833	480	2.58	0.80	9.1	16.3	24.4	3.4	5.1	0.17	7.7	236	

[a] In butyronitrile at 77 K; observed absorption maxima, maxima for Gaussian fitting functions for [**11**−**18**][PF_6]$_2$ in brackets. Data in all subsequent columns relate to fitted curves if used. [b] For [**3**−**10**][PF_6]$_2$, obtained from $(4.32 \times 10^{-9}$ M $cm^2)A$ where A is the numerically integrated area under the absorption peak; for [**11**−**18**][PF_6]$_2$, obtained from $(4.60 \times 10^{-9}$ M $cm^2)\varepsilon_{max} \times fw_{1/2}$, where ε_{max} is the maximal molar extinction coefficient and $fw_{1/2}$ is the full width at half height (in wavenumbers). [c] Calculated using eq 2. [d] Calculated from $f_{int}\Delta\mu_{12}$ using $f_{int} = 1.33$. [e] Calculated from eq 1. [f] Delocalized electron-transfer distance calculated from $\Delta\mu_{12}/e$. [g] Effective (localized) electron-transfer distance calculated from $\Delta\mu_{ab}/e$. [h] Calculated from eq 3. [i] Calculated from eq 4. [j] Calculated from eq 5. [k] Data taken in part from ref 13. [l] Data taken in part from ref 8c.

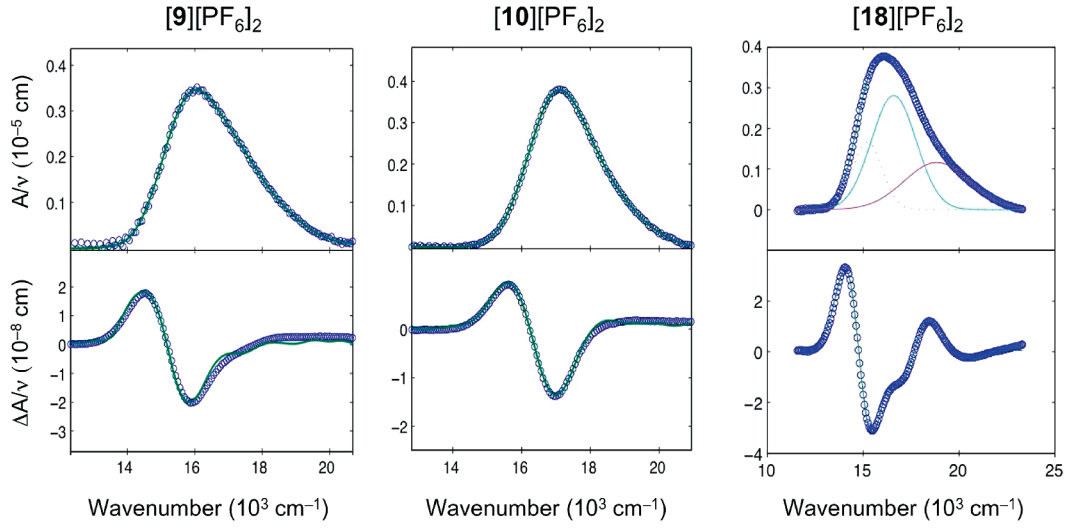

Figure 9. Stark spectra and calculated fits for salts [**9**][PF_6]$_2$, [**10**][PF_6]$_2$, and [**18**][PF_6]$_2$ in an external electric field of 3.51×10^7 V m^{-1}. (Top panel) Absorption spectrum illustrating Gaussian curves used in data fitting for [**18**][PF_6]$_2$. (Bottom panel) Electroabsorption spectrum, experimental (blue) and fits (green) according to the Liptay equation.[27a]

Given the strongly limited validity of the β_0 values derived via HRS data (see above), due to resonance and the inherent complexity of the chromophores under study, and the fact that no other direct experimental method for determining such data exists, Stark measurements provide a useful means to assess the intrinsic NLO responses of our new molecules. Therefore, β_0 values have been estimated by using eq 5 (Table 6). It should be emphasized that the two-state model is applied in a different sense here when compared with the HRS studies. The latter are inherently able to probe only the NLO responses of *whole*

chromophores, while in contrast, the Stark observations allow the system to be broken down into its component electronic excitation processes which may be viewed as having two-state nature. While including the important benefit of completely avoiding complications due to resonance effects, this indirect analytical approach is nevertheless only an approximation that involves three assumptions: (i) all of the visible absorption arises from ICT transitions, so that even if a band is resolved into components, each of these can be adequately described as involving a ground and single excited state; (ii) each Gaussian curve corresponds with a single ICT process; (iii) the relative directionality of μ_{12} is not important in the two-state model.[25] Assumption (ii) may be somewhat tentative given that the TD-DFT calculations (see below) predict up to 5 ICT transitions of substantial intensity for some of the DS species, but experimentally this represents a "best case approximation" scenario. Literature precedent indicates that assumption (iii) is reasonable (see eqs 40 and 41 in ref 6a).[28]

For [**11**−**18**][PF_6]$_2$, the total NLO response ($\Sigma\beta_0$) is taken as the sum of those for the Gaussian curves. Notably, related studies have shown that using such an approach usually gives total β_0 values similar to those obtained without spectral deconvolution.[18,29] It is also important to note that other two-state descriptions exist, which would change the quoted β_0 values by constant factors of 0.5 or 2.[30] Therefore, these data are useful primarily for revealing structure−activity relationships, rather than necessarily indicating the *absolute magnitudes* of β_0. Nevertheless, it is remarkable that previous studies with 1D Ru^{II} complexes show that using the two-state eq 5 with a prefactor of 3 (the "perturbation series convention")[30] often gives excellent quantitative agreement with the β_0 values determined via HRS with a 1064 nm laser.[31] Although the general applicability of this basic two-state model is certainly limited and refinements have been proposed,[32] recent theoretical studies confirm that good estimates of β_0 can be obtained for 1D dipoles via even such a simplified approach.[33] Furthermore, previous experimental observations such as our own[31] show that eq 5 remains a viable tool when considering the molecular NLO responses associated with single ICT transitions. The novelty of the present study lies in extending our Stark-based treatment to more complicated 2D systems, following the original precedent set by Vance and Hupp.[7e] While we acknowledge that our approach is only an approximation from a physical perspective, the fact that treating all the compounds in the same manner affords consistent and plausible trends (see below) lends further credence to the results.

The Stark-derived β_0 values show several very clear trends, reinforcing those noted in the HRS data (see above). First, extending the π-conjugation always markedly increases β_0, with the largest (ca. 2-fold) change for the pair [**9**/**10**][PF_6]$_2$. Such behavior is expected by comparison with simpler organic molecules,[1] and attributable to mainly the combination of decreasing E_{max} and increasing $\Delta\mu_{12}$ values (Table 6). Interestingly, the largest relative β_0 increases are found for the MS compounds. Our previous studies with 1D pyridinium and related species showed that replacing Dap with the stronger π-ED group Jd usually (and logically) increases β_0.[18] A similar pattern is observed for the diquat compounds, although the difference is not significant for the pair [**11**/**13**][PF_6]$_2$. For the other seven pairs, the increases in β_0 lie in the range ca. 20−70%, and are largely due to the decreases in E_{max}. In contrast, the β_0 responses of the EDQ^{2+}/PDQ^{2+} pairs do not differ significantly, because the blue-shifting of the ICT transitions on extending the quaternized bridge is offset by their increased intensities. The most substantial increases in β_0 (ca. 45−195%) are generally observed on moving from a MS compound to its DS counterpart. This trend is attributable primarily to the greatly increased μ_{12} values for the DS chromophores (see above).

Since DAST is now a technologically valuable material, it is important to compare the NLO responses of our new chromophores with that of the DAS^+ cation. Many of the diquat-based salts show HRS-derived β_0 values larger than that of [DAS]PF_6,[8b,c] with the value for [**18**][PF_6]$_2$ being about 3 times larger (Table 5). However, given the limitations introduced by resonance effects and electronic structural differences in these HRS data, it is probably more instructive to draw comparisons using the Stark-derived results. By using this approach, we obtained a β_0 value for [DAS]PF_6 that is significantly smaller than any of those derived for the new compounds (Table 6). Indeed, the $\Sigma\beta_0$ responses estimated for [**12**][PF_6]$_2$, [**14**][PF_6]$_2$, [**16**][PF_6]$_2$, and [**18**][PF_6]$_2$ are ca. 5−6-fold increased when compared with [DAS]PF_6. These observations provide a strong incentive to pursue studies on polar materials incorporating these new symmetrical diquat cations, such as [**15**][$NapSO_3$]$_2$·$2H_2O$ (see above), in which exceptionally large and 2D bulk NLO effects may be anticipated.

Theoretical Studies. The electronic structures of a selection of the new diquat chromophores (**3**, **7**, **11**, **12**, **14**−**16**, and **18**) have been studied by using density functional theory (DFT) methods. These calculations give py/py angles of 48−51° in the PDQ^{2+} derivatives, while smaller twists of 23−24° are predicted for the EDQ^{2+} species. The latter are only a little smaller than the value determined crystallographically for the salt [**13**][OTf]$_2$·2MeCN (Table 4), while the predictions for the PDQ^{2+} species are close to the average angle (52.9°) observed for the eight crystal structures we report. The parameters involved in eq 5 were determined by time-dependent DFT (TD-DFT) calculations, and β values were calculated from the numerical second derivative of the dipole moment with respect to the applied electric field by using the finite field (FF) approach. The results of these calculations are shown in Table 7. While a recent comparative study of quantum mechanical methods for predicting β_0 (including FF-DFT) concluded that such approaches are relatively reliable for pseudolinear dipoles,[34]

(28) Coe, B. J.; Harris, J. A.; Jones, L. A.; Brunschwig, B. S.; Song, K.; Clays, K.; Garín, J.; Orduna, J.; Coles, S. J.; Hursthouse, M. B. *J. Am. Chem. Soc.* **2005**, *127*, 4845–4859.
(29) Coe, B. J.; Foxon, S. P.; Harper, E. C.; Helliwell, M.; Raftery, J.; Swanson, C. A.; Brunschwig, B. S.; Clays, K.; Franz, E.; Garín, J.; Orduna, J.; Horton, P. N.; Hursthouse, M. B. *J. Am. Chem. Soc.* **2010**, *132*, 1706–1723.
(30) Willetts, A.; Rice, J. E.; Burland, D. M.; Shelton, D. P. *J. Chem. Phys.* **1992**, *97*, 7590–7599.
(31) Coe, B. J.; Harris, J. A.; Brunschwig, B. S. *J. Phys. Chem. A* **2002**, *106*, 897–905.
(32) Selected examples: (a) Meshulam, G.; Berkovic, G.; Kotler, Z. *Opt. Lett.* **2001**, *26*, 30–32. (b) Woodford, J. N.; Wang, C. H.; Jen, A. K.-Y. *Chem. Phys.* **2001**, *271*, 137–143. (c) Di Bella, S. *New J. Chem.* **2002**, *26*, 495–497. (d) Tai, O. Y.-H.; Wang, C. H.; Ma, H.; Jen, A. K.-Y. *J. Chem. Phys.* **2004**, *121*, 6086–6092. (e) Kuzyk, M. G. *Phys. Rev. A* **2005**, *72*, 053819-1–053819-5. (f) Campo, J.; Wenseleers, W.; Goovaerts, E.; Szablewski, M.; Cross, G. H. *J. Phys. Chem. C* **2008**, *112*, 287–296.
(33) Champagne, B.; Kirtman, B. *J. Chem. Phys.* **2006**, *125*, 024101-1–024101-7.
(34) Isborn, C. M.; Leclercq, A.; Vila, F. D.; Dalton, L. R.; Brédas, J. L.; Eichinger, B. E.; Robinson, B. H. *J. Phys. Chem. A* **2007**, *111*, 1319–1327.

Table 7. Calculated Electronic Transitions (TD-B3P86/6-31G*) and Finite Field Hyperpolarizabilities for the Diquat Cations **3**, **7**, **11**, **12**, **14**−**16**, and **18** and DAS^+

cation	E_{max}[a] (eV)	symmetry[a]	μ_{12}[a] (D)	f_{os}[a]	$\Delta\mu_{12}$[a,b] (D)	major contributions[a]	β_{zzz}[c] (10^{-30} esu)	β_{zyy}[c] (10^{-30} esu)	$\Sigma[\beta_{FF}]$[c] (10^{-30} esu)	β_{zyy}/β_{zzz}
3	1.45		6.61	0.24	26.07	H → L			277	
	2.69		11.52	1.35	7.83	H → L+1				
7	1.51		5.98	0.20	32.17	H → L			407	
	2.34		5.76	0.30	33.36	H → L+1				
	2.79		10.55	1.18	12.67	H → L+2				
11	1.73	*B*	10.66	0.75	10.64	H → L	64	289	353	4.5
	1.86	*A*	3.86	0.11	10.53	H−1 → L				
	2.59	*B*	6.93	0.47	8.10	H−1 → L+1				
	2.68	*A*	6.25	0.40	11.13	H → L+1				
	2.77	*B*	7.29	0.56	14.06	H → L+2				
	2.95	*A*	9.26	0.96	10.56	H−1 → L+2				
12	1.58	*B*	14.06	1.18	10.45	H → L	88	527	615	6.0
	1.70	*A*	3.68	0.09	10.47	H−1 → L				
	2.31	*B*	9.98	0.87	6.95	H−1 → L+1				
	2.47	*A*	8.81	0.73	10.78	H → L+1				
	2.57	*B*	7.81	0.60	14.60	H → L+2				
	2.72	*A*	9.28	0.89	10.68	H−1 → L+2				
14	1.53	*B*	14.82	1.27	9.90	H → L	78	573	650	7.3
	1.64	*A*	3.53	0.08	9.88	H−1 → L				
	2.25	*B*	9.97	0.85	6.35	H−1 → L+1				
	2.41	*A*	8.95	0.73	10.43	H → L+1				
	2.51	*B*	7.96	0.60	14.38	H → L+2				
	2.66	*A*	9.65	0.94	9.62	H−1 → L+2				
15	1.87	*B*	8.75	0.54	9.98	H → L	56	213	269	3.8
	1.95	*A*	2.90	0.06	9.82	H−1 → L				
	2.50	*B*	11.06	1.16	7.08	H−1 → L+1				
	2.72	*A*	9.39	0.91	8.94	H → L+1				
16	1.69	*B*	11.18	0.80	9.79	H → L	80	382	462	4.8
	1.76	*A*	2.70	0.05	9.69	H−1 → L				
	2.24	*B*	14.25	1.72	6.60	H−1 → L+1				
	2.50	*A*	11.38	1.23	9.12	H → L+1				
	2.84	*B*	5.18	0.29	14.53	H → L+2				
	2.89	*A*	5.29	0.31	12.44	H−1 → L+2				
18	1.63	*B*	11.72	0.85	9.20	H → L	75	408	482	5.4
	1.70	*A*	2.56	0.04	9.09	H−1 → L				
	2.17	*B*	14.64	1.77	5.91	H−1 → L+1				
	2.45	*A*	11.72	1.28	8.32	H → L+1				
	2.77	*B*	5.13	0.28	14.38	H → L+2				
	2.82	*A*	5.38	0.31	11.92	H−1 → L+2				
DAS^{+}[d]	2.65		11.5	1.32	13.9	H → L			150	

[a] TD-B3P86/6-31G*, only transitions with excitation energies below 3.0 eV are included; H = HOMO, L = LUMO. [b] Derived from the excited state dipole moment calculated by using the RhoCI density. [c] Static hyperpolarizability calculated by using FF-B3P86/6-31G*. [d] Data taken from ref 8d (B3P86/LanL2DZ model Chemistry).

we note that the FF-DFT method has been applied only rarely to 2D species.[6p,13,28,29]

The MS cations **3** and **7** resemble stilbazolium species, with lowest energy (LE) electronic transitions of HOMO → LUMO character.[8e] Figures S8 and S9 (Supporting Information) show the topologies of the MOs involved. In each case, the HOMO is primarily Dap-based, but with significant contributions from the ethenyl bridge and attached pyridyl ring. The LUMO is located mostly on the diquat units (and especially the picolyl ring), while the LUMO+1 and LUMO+2 also feature some contributions from the rest of the molecule. TD-DFT does not accurately predict the observed ICT energies (Tables 2 and 6), underestimating E_{max} by ca. 0.7−0.8 eV, but the trend of E_{max} increasing on replacing EDQ^{2+} with PDQ^{2+} is reproduced. These calculations indicate that both the HOMO and LUMO are destabilized on moving from **3** to **7**, but this effect is larger for the LUMO. The second lowest energy (SLE) transition predicted has HOMO → LUMO+1 character for both cations, with an E_{max} somewhat closer to (but higher than) the experimental value. However, these transitions show a reverse trend of decreasing E_{max} on moving from **3** to **7**. The predicted values of μ_{12} and $\Delta\mu_{12}$ for the LE transitions agree only moderately with those measured at 77 K (Table 6). The FF-DFT-derived β_0 (β_{FF}) values are very large and show a substantial increase for the PDQ^{2+} derivative when compared with its EDQ^{2+} analogue. This result contrasts with the HRS and Stark studies which afford very similar β_0 values for [**3**][PF_6]$_2$ and [**7**][PF_6]$_2$ (Tables 5 and 6). For comparison, the DAS^+ cation gives $\beta_{FF} = 150 \times 10^{-30}$ esu,[8d] confirming the expected enhancements for the new diquat chromophores. This result provides confirmation of the (at least approximate) validity of our experimentally derived β_0 data because the FF method calculates the first hyperpolarizability as the second derivative of the dipole moment with respect to an applied electric field, and is completely independent of any potential concerns over the applicability of the two-state model.

The overall picture arising from our calculations on the six DS cations is similar to that described previously for V-shaped Ru^{II} complexes.[28,29] Thus, all of the chromophores have C_2 symmetry and their MOs are symmetric (a) or antisymmetric (b) with respect to the 2-fold axis (z in the standard orientation). The electronic transitions between orbitals with the same symmetry (*A* transitions) are polarized along the z axis and contribute to the β_{zzz} tensor component, while the transitions

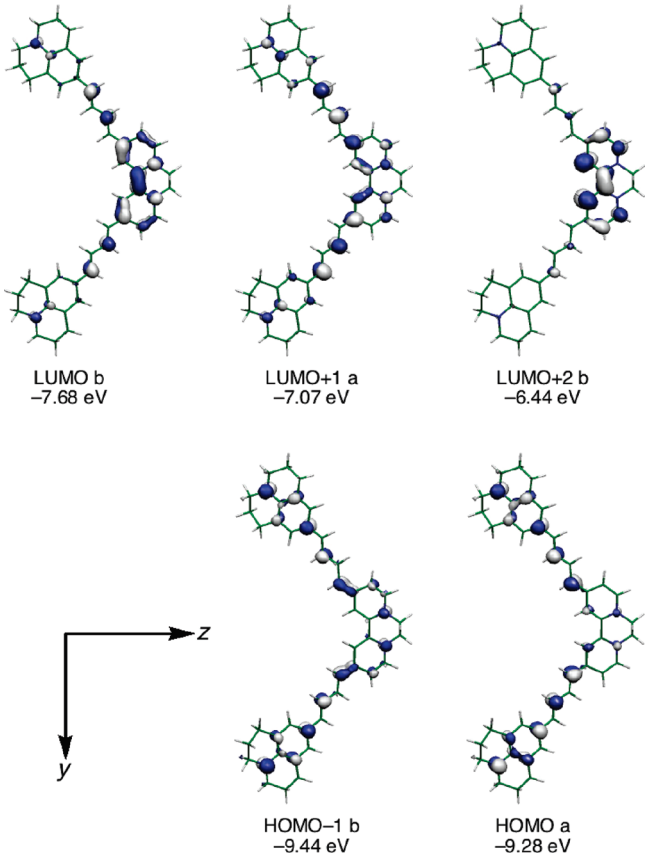

Figure 10. Illustrations of the contour surface diagrams of the molecular orbitals of **14** involved in the six lowest energy transitions (isosurface value 0.04 au), showing the axis convention used in all of the calculations.

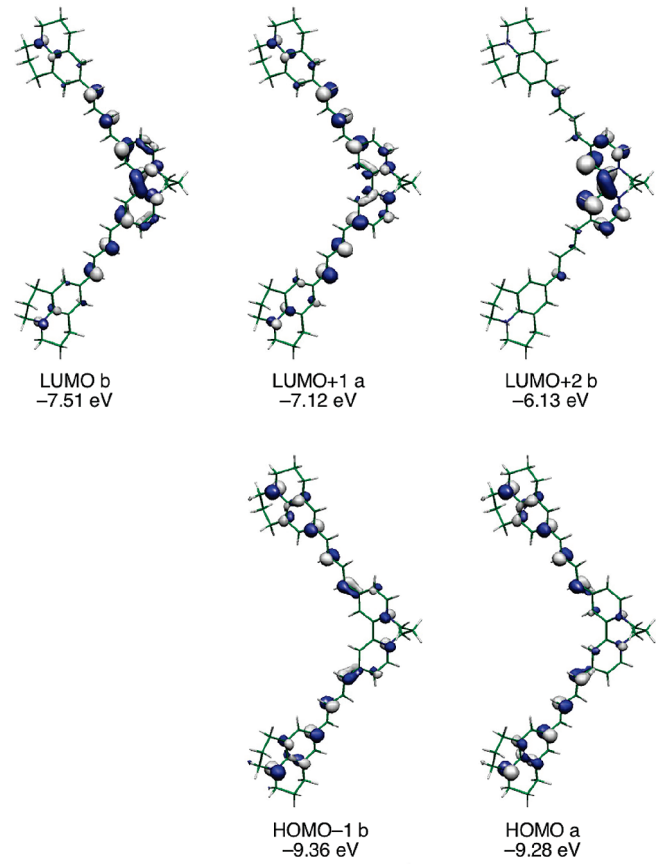

Figure 11. Illustrations of the contour surface diagrams of the molecular orbitals of **18** involved in the six lowest energy transitions (isosurface value 0.04 au).

between orbitals with different symmetries (*B* transitions) are polarized perpendicular to the *z* axis and therefore contribute to β_{zyy}.

The calculated electronic structures and excitation properties of **11**, **12**, **14**−**16**, and **18** are rather more complicated than for **3** and **7**. For each cation, the LE transition is again of HOMO → LUMO character and *B*-polarized, but an *A*-polarized SLE (HOMO−1 → LUMO) transition is also predicted, with E_{max} being only ca. 0.1 eV above that of the LE transition (Table 7). Another pair of transitions appears at rather higher energies; a *B*-polarized HOMO−1 → LUMO+1 and an *A*-polarized HOMO → LUMO+1, separated by 0.07−0.28 eV. For all of the chromophores except **15**, a third pair of transitions 0.05−0.18 eV apart is predicted at even higher energies (*B*-polarized HOMO → LUMO+2 and *A*-polarized HOMO−1 → LUMO+2). Figures 10 and 11 show the topologies of the MOs involved for **14** and **18**, while the corresponding diagrams for the other species are included in the Supporting Information (Figures S10−S13). The HOMO and HOMO−1 are always mostly located on the electron-rich Dap or Jd phenyl groups, but with significant contributions from the ethenyl/butadienyl bridges and the diquat units. The LUMO, LUMO+1 and LUMO+2 are concentrated on the electron-accepting diquat fragments, with the LUMO+2 having especially limited contributions from the rest of the molecule. In qualitative terms, the electronic structure is not greatly influenced by the various structural changes made.

As for **3** and **7**, the TD-DFT E_{max} values for the LE and SLE transitions in **11**, **12**, **14**−**16**, and **18** are somewhat lower than those measured experimentally (Tables 2 and 6). However, the empirical trends in ICT energies are all predicted by these calculations. Thus, E_{max} for both transitions decreases on moving from $n = 1$ to 2 (pairs **11/12** and **15/16**) or on replacing Dap with Jd (pairs **12/14** and **16/18**), but increases on moving from an EDQ^{2+} derivative to its PDQ^{2+} counterpart (pairs **11/15**, **12/16**, and **14/18**). While the measurements show only small increases in E_{max} ($\leq$0.06 eV) for the DS species when compared with their MS analogues, more significant increases are predicted for the LE transition energies of the pairs **3/11** (0.28 eV) and **7/15** (0.36 eV). Again, the extent of agreement between the predicted and measured values of μ_{12} and $\Delta\mu_{12}$ (Table 6) is generally poor, and in particular, the TD-DFT-derived $\Delta\mu_{12}$ values are all 2−3 times smaller than those determined from the Stark studies and also those predicted for **3** and **7**.

The main point of note concerning the FF-DFT-derived β values is that the off-diagonal tensor component β_{zyy} is always larger than β_{zzz}, by a factor of ca. 4−7. Coupled perturbed Hartree−Fock calculations on **11** predicted the same general behavior,[13] although according to this method the β_{zyy}/β_{zzz} ratio is smaller (2.1) than that derived via FF-DFT (4.5). The results for the pairs **11/12** and **15/16** indicate that the relative dominance of β_{zyy} increases as the π-conjugation extends. Furthermore, the ratio β_{zyy}/β_{zzz} also increases on replacing Dap with Jd (pairs **12/14** and **16/18**), but decreases on moving from an EDQ^{2+} derivative to its PDQ^{2+} analogue (pairs **11/15**, **12/16**, and **14/18**). The Dap vs Jd trend, but only this one, is also shown by the HRS data (Table 5).

When considering the total FF-DFT-derived β_0 ($\Sigma[\beta_{FF}]$) values, the following trends are predicted: (i) $\Sigma[\beta_{FF}]$ increases on moving from $n = 1$ to 2, or on replacing Dap with Jd, but

the effect of the latter change is much less significant; (ii) $\Sigma[\beta_{FF}]$ decreases on moving from an EDQ^{2+} derivative to its PDQ^{2+} counterpart for the DS pairs **11/15**, **12/16**, and **14/18**, but the opposite is found for the MS pair **3/7**. These predictions generally agree qualitatively with the conclusions from the Stark studies (see above), providing further validation of our experimental approach, but the EDQ^{2+} vs PDQ^{2+} comparisons are more clear-cut according to FF-DFT. However, the effect of moving from a MS derivative to its DS counterpart is not reproduced consistently. While the Stark results indicate that this change always markedly increases the total β_0 response, the FF-DFT results show an increase in moving from **3** to **11**, but a decrease for the pair **7/15**.

Conclusion

We have synthesized the first family of diquat-based NLO chromophores. Their visible absorption spectra are dominated by intense ICT bands, the energies of which show both predictable (Dap vs Jd, $n = 1 \rightarrow 2$) and previously unobserved (MS vs DS, EDQ^{2+} vs PDQ^{2+}) trends. Cyclic voltammograms show two reversible diquat-based reductions, and single-crystal X-ray structures have been determined for nine salts. HRS studies with an 800 nm laser reveal relatively large β responses, with depolarization experiments showing dominant 'off-diagonal' β_{zyy} tensor components for the DS compounds. Stark spectroscopy allows the estimation of β_0 values in the absence of complications arising from the variable effects of resonance, and affords structure−activity correlations according to the two-state model. The main new insights emerging from the Stark-based analyses are that the β_0 responses of the EDQ^{2+} and PDQ^{2+} pairs do not differ significantly, and the largest increases in β_0 occur on moving from a MS species to its DS counterpart. TD-DFT computations on selected chromophores reveal a relatively high multiplicity of visible ICT transitions for the DS species. FF-DFT calculations predict for the DS chromophores that β_{zyy} is always larger than β_{zzz}, by a factor of ca. 4−7. In terms of the trends in the total β responses, the FF-DFT approach also gives a generally good qualitative level of agreement with the Stark studies. In addition to these detailed insights, our studies afford several conclusions of potentially wide-reaching significance. First, β_0 values ca. 6 times larger than that of the chromophore in the commercial NLO material (*E*)-4′-(dimethylamino)-*N*-methyl-4-stilbazolium tosylate are achieved, by joining two π-EDS to a powerful diquat acceptor. Second, the new species have strongly 2D NLO responses that may be exploited for novel practical applications. Third, we have demonstrated that such chromophores can form polar crystalline materials, suitable for bulk NLO behavior. Finally, the presence of two reversible reductions indicates potential for redox-switchability over multiple states. Notably, redox-switching of NLO responses has been achieved hitherto only with transition metal complexes.[35]

Acknowledgment. We thank the EPSRC for support (Grants EP/E000738 and EP/D070732) and also the Fund for Scientific Research-Flanders (FWO-V, G.0297.04), the University of Leuven (GOA/2006/3), MCyT-FEDER (CTQ2005-01368, CTQ2008-02942), the NSF (Grant CHE-0802907, 'Powering the Planet: an NSF Center for Chemical Innovation') and Gobierno de Aragon-Fondo Social Europeo (E39). We thank Dr. Emma C. Fitzgerald for assistance with obtaining the data for Figure 4, Kurt De Mey for assistance with the HRS studies, and Dr. John E. Warren (Synchrotron Radiation Source, CCLRC, Daresbury Laboratory, Warrington WA4 4AD, U.K.) for assistance with the data collection for [**16**][$NapSO_3$]$_2$·$2H_2O$ and [**18**][PF_6]$_2$·$2Me_2CO$.

Supporting Information Available: Experimental details; additional ^{1}H NMR figure; further crystallographic data and figures; X-ray powder diffraction data for [**15**][$NapSO_3$]$_2$·$2H_2O$; crystallographic information in CIF format, including [**7**][$NapSO_3$]$_2$, [**7**][PF_6]$_2$·MeCN, and [**9**][PF_6]$_2$·MeCN; method for derivation of β components from HRS data; Cartesian coordinates of theoretically optimized geometries for the cations **3**, **7**, **11**, **12**, **14**−**16**, and **18**; contour surface diagrams of the MOs involved in the lowest energy transitions for the cations **3**, **7**, **11**, **12**, **15**, and **16**. This material is available free of charge via the Internet at http://pubs.acs.org.

JA103289A

(35) Selected examples: (a) Coe, B. J.; Houbrechts, S.; Asselberghs, I.; Persoons, A. *Angew. Chem., Int. Ed.* **1999**, *38*, 366–369. (b) Weyland, T.; Ledoux, I.; Brasselet, S.; Zyss, J.; Lapinte, C. *Organometallics* **2000**, *19*, 5235–5237. (c) Malaun, M.; Reeves, Z. R.; Paul, R. L.; Jeffery, J. C.; McCleverty, J. A.; Ward, M. D.; Asselberghs, I.; Clays, K.; Persoons, A. *Chem. Commun.* **2001**, 49–50. (d) Powell, C. E.; Cifuentes, M. P.; Morrall, J. P.; Stranger, R.; Humphrey, M. G.; Samoc, M.; Luther-Davies, B.; Heath, G. A. *J. Am. Chem. Soc.* **2003**, *125*, 602–610. (e) Sporer, C.; Ratera, I.; Ruiz-Molina, D.; Zhao, Y.-X.; Vidal-Gancedo, J.; Wurst, K.; Jaitner, P.; Clays, K.; Persoons, A.; Rovira, C.; Veciana, J. *Angew. Chem., Int. Ed.* **2004**, *43*, 5266–5268. (f) Cifuentes, M. P.; Powell, C. E.; Morrall, J. P.; McDonagh, A. M.; Lucas, N. T.; Humphrey, M. G.; Samoc, M.; Houbrechts, S.; Asselberghs, I.; Clays, K.; Persoons, A.; Isoshima, T. *J. Am. Chem. Soc.* **2006**, *128*, 10819–10832. (g) Boubekeur-Lecaque, L.; Coe, B. J.; Clays, K.; Foerier, S.; Verbiest, T.; Asselberghs, I. *J. Am. Chem. Soc.* **2008**, *130*, 3286–3287.